

1 **Transport of short-lived halocarbons to the stratosphere over the**
2 **Pacific Ocean.**

3 Michal T. Filus¹, Elliot L. Atlas², Maria A. Navarro^{2*}, Elena Meneguz³, David Thomson³, Matthew J.
4 Ashfold⁴, Lucy J. Carpenter⁵, Stephen J. Andrews⁵, Neil R.P. Harris⁶

- 5
6 1. Centre for Atmospheric Science, University of Cambridge, Cambridge, CB2 1EW, UK
7 2. Department of Atmospheric Sciences, RSMAS, University of Miami, Miami, Florida, USA
8 3. Met Office, Atmospheric Dispersion Group, FitzRoy Road, Exeter, EX1 3PB, UK
9 4. School of Environmental and Geographical Sciences, University of Nottingham Malaysia
10 Campus, 43500, Semenyih, Selangor, Malaysia
11 5. Wolfson Atmospheric Chemistry Laboratories, Department of Chemistry, University of York,
12 York, YO10 5DD, UK
13 6. Centre for Environmental and Agricultural Informatics, Cranfield University, Cranfield, MK43
14 0AL, UK

15
16 *Correspondence to:* Neil Harris (neil.harris@cranfield.ac.uk)

17 **Abstract.** The effectiveness of transport of short-lived halocarbons to the upper troposphere and
18 lower stratosphere remains an important unknown-uncertainty in quantifying the supply of ozone-
19 depleting substances to the stratosphere. In early 2014, a major field campaign in Guam in the West
20 Pacific, involving UK and US research aircraft, sampled the tropical troposphere and lower
21 stratosphere. The resulting measurements of CH₃I, CHBr₃ and CH₂Br₂ are compared here with
22 calculations from a Lagrangian model. This methodology benefits from an updated convection
23 scheme which improves simulation of the effect of deep convective motions on particle distribution
24 within the tropical troposphere. We find that the observed CH₃I, CHBr₃ and CH₂Br₂ mixing ratios in
25 the Tropical Tropopause Layer (TTL) are consistent with those in the boundary layer when the new
26 convection scheme is used to account for convective transport. Particularly More specifically,
27 comparisons between modelled estimates and observations of short~~est~~-lived CH₃I indicates that the
28 updated NAME-convection scheme is realistic up to the lower TTL but is less good at reproducing
29 the small number of extreme convective events in the upper TTL. This study consolidates our
30 understanding of the transport of short-lived halocarbons to the upper troposphere and lower
31 stratosphere by using improved model calculations to confirm consistency between observations in
32 the boundary layer, observations in the TTL, and atmospheric transport processes. Our results
33 support recent estimates of the contribution of short-lived bromocarbons to the stratospheric bromine
34 budget.

35
36 **1 Introduction**

37 The successful implementation of the Montreal Protocol with its adjustments and amendments has
38 led to reductions in stratospheric chlorine and bromine amounts since the late 1990s (Carpenter et al.,
39 2014). These reductions have halted the ozone decrease (Harris et al., 2015; Chipperfield et al., 2017;
40 Steinbrecht et al., 2017) with the exception of the possible continued reducedepletion in the lower
41 stratosphere (Ball et al., 2017; Chipperfield et al., 2018; Ball et al., 2019). Recently, the importance
42 of very short-lived (VSL) chlorine- and bromine containing compounds has received a great deal of

Formatted: Space After: 6 pt

Formatted: Font: 12 pt

Formatted: Space Before: 0 pt, After: 6 pt

Formatted: Space After: 6 pt

Formatted: Indent: Left: 0 cm, First line: 0 cm, Space After: 6 pt

Formatted: Font: 12 pt

Formatted: Font: 12 pt

Formatted: Font: 12 pt

Formatted: Font: 12 pt

Formatted: Font: 12 pt

Formatted: Space After: 6 pt

Field Code Changed

Formatted: Font: 12 pt

Formatted: Font: 12 pt

Formatted: Font: 12 pt

Formatted: Space After: 6 pt, Line spacing: Multiple 1.15 li

Formatted: Font: 12 pt

Formatted: Font: 12 pt

Formatted: Line spacing: Multiple 1.15 li

Formatted: Space After: 6 pt, Line spacing: Multiple 1.15 li

Formatted: Font: 12 pt

Formatted: Font: 12 pt

Formatted: Font: 12 pt

*Deceased: 19.12.2017

43 attention (e.g. Hossaini et al., 2017; Oram et al., 2017). VSLs are not ~~considered-controlled~~ under
44 the Montreal Protocol, but are required in order to ~~ensure~~ reconcile ~~between~~ observed stratospheric
45 measurements of inorganic or 'active' bromine with reported anthropogenic bromine emission
46 sources. ~~However~~ VSLs input into the stratosphere has ~~however~~ remained a poorly constrained
47 quantity (Carpenter et al., 2014), which hinders our understanding of the on-going decline in lower
48 stratospheric ozone and our ability to make predictions of stratospheric ozone recovery.

Formatted: Font: 12 pt

49 Three of the most important VSL halocarbons are: ~~methyl iodide~~, CH_3I ; ~~bromoform~~, CHBr_3 ; and
50 ~~dibromomethane~~, CH_2Br_2 . They have typical lower tropospheric lifetimes (4, 15 and 94 days,
51 respectively (Carpenter et al., 2014)) which are shorter than tropospheric transport timescales and so
52 they have non-uniform tropospheric abundances. They are ~~all~~ emitted predominantly from the oceans
53 and result principally from natural sources (e.g. Lovelock, 1975; ~~Moore et al., 1995; Solomon et al.,~~
54 ~~1994;~~ Oram and Penkett, 1994; Vogt et al., 1999; ~~Salawitch et al., 2006;~~ Pyle et al., 2011; Carpenter
55 et al., ~~1999,~~ 2012, 2014; Tegtmeier et al., 2013; Saiz-Lopez et al., 2014). The short-lived
56 bromocarbons, chiefly CHBr_3 and CH_2Br_2 , have been identified as the missing source for ~~the~~
57 stratospheric ~~active~~ bromine (~~mostly originating the sum of from bromine atoms in~~ long-lived
58 brominated organic and inorganic substances; Pfeilsticker et al., 2000; ~~Salawitch, 2006;~~ Feng et al.,
59 2007; Dessens et al., 2009). The current estimates of the contribution of the short-lived
60 bromocarbons to the active bromine (Br_y) in the stratosphere ~~is ~5 (3-7) ppt (Engel et al., 2018),~~
61 ~~which is slightly narrower than the previous range from of~~ 3-8 ppt (Liang et al., 2010, 2014;
62 Carpenter et al., 2014; Fernandez et al., 2014; Sala et al., 2014; Tegtmeier et al., 2015; Navarro et al.,
63 2015, 2017; Hossaini et al., 2016; Butler et al., 2017; Fiehn et al., 2017). Much of ~~this the~~ uncertainty
64 is linked to the contribution of CHBr_3 which has both the shortest lifetime and the largest emissions
65 of the commonly observed bromocarbons.

Formatted: Font: 12 pt

Formatted: Font: 12 pt

Formatted: Font: 12 pt

Formatted: Font: 12 pt

Formatted: Font: 12 pt

Formatted: Font: 12 pt

Formatted: Font: 12 pt

Formatted: Font: 12 pt

Formatted: Font: 12 pt

Formatted: Font: 12 pt

66 The transport of VSL halocarbons into the lower stratosphere is by ascent through the tropical
67 tropopause layer (TTL) (Fueglistaler et al., 2009). An important factor influencing the loading of the
68 VSL bromocarbons in the TTL is the strength of the convective transport from the boundary layer
69 where the bromocarbons are emitted (Hosking et al., 2010; ~~Yang et al., 2014;~~ Russo et al., 2015;
70 ~~Hepach et al., 2015;~~ Fuhlbrügge et al., 2016; Krzysztofiak et al., 2018). This is poorly quantified and,
71 ~~especially~~ when taken together with the large variations in boundary layer concentrations and the
72 ~~uncertainties associated with the model representation of convection parameterisation being the~~
73 ~~major source of uncertainty in chemistry transport models~~, limits our ability to model the bromine
74 budget in the current and future atmosphere (Liang et al., 2010, 2014; Hoyle et al., 2011; Russo et
75 al., 2011, 2015; Schofield et al., 2011; Aschmann et al., 2013; Fernandez et al., 2014; Hossaini et al.,
76 2016; Krzysztofiak et al., 2018).

Formatted: Font: 12 pt

77 To address this and other challenges, the Natural Environment Research Council Coordinated
78 Airborne Studies in the Tropics (NERC CAST), National Centre for Atmospheric Research
79 Convective Transport of Active Species in the Tropics (NCAR CONTRAST) and National
80 Aeronautics and Space Administration Airborne Tropical Tropopause Experiment (NASA
81 ATTREX) projects were organised (Harris et al., 2017; Jensen et al., 2017; Pan et al., 2017). These
82 projects joined forces in January-March 2014 in the American territory of Guam, in the West Pacific.
83 Three aircraft were deployed to sample air masses at different altitudes to investigate the
84 characteristics of ~~the air~~ masses ~~affected-influenced by the deep convection~~ systems. This
85 campaign produced a unique dataset of coordinated measurements for interpretative studies of
86 transport and distribution of the chemical species, including the VSL bromocarbons (Sect. 2.1 and

Formatted: Font: 12 pt

Formatted: Font: 12 pt

Formatted: Font: 12 pt

87 2.2). The NASA ATTREX project also measured over the less convectively active east Pacific in
 88 January - February 2013.

89 The objective of this paper is to model the transport and distribution of CH₃I, CHBr₃ and CH₂Br₂ in
 90 the TTL by quantifying their boundary layer and background contribution components using a ~~new~~
 91 Lagrangian methodology building on the approach of Ashfold et al (2012). A new parameterisation
 92 scheme of convection for the NAME trajectory model is used with the short-lived CH₃I serving as an
 93 excellent way to assess the performance of the new scheme. Briefly, the approach uses clusters of
 94 back trajectories starting at measurement points to quantify how much of CH₃I, CHBr₃ and
 95 CH₂Br₂ in the TTL come from the boundary layer, ~~and thereby~~ assessing the role of convection in
 96 transporting these compounds to the TTL. The calculation is completed by estimating the
 97 background component (i.e. how much of CH₃I, CHBr₃ and CH₂Br₂ originate from outside the
 98 immediate boundary layer source). Section 2 presents an overview of the field campaigns, the CH₃I,
 99 CHBr₃ and CH₂Br₂ measurements, and how the NAME calculations are used. In Section 3, the
 100 approach is illustrated by comparing model estimates and measurements from one ATTREX 2014
 101 flight. This analysis is then expanded to cover measurements from all ATTREX 2014 and 2013
 102 flights. The role of convection in transporting VSL halocarbons to the TTL is further examined in
 103 Section 4. Based on the modelled calculations of CHBr₃ and CH₂Br₂, Section 5 discusses how much
 104 these VSL bromocarbons contribute to the bromine budget in the TTL.

105 **2 Methodology**

106 **2.1 Overview of the CAST, CONTRAST and ATTREX campaigns**

107 The joint CAST, CONTRAST and the third stage of the ATTREX campaign took place in January-
 108 March 2014, in the West Pacific. Guam (144.5° E, 13.5° N) was used as a research mission centre for
 109 these three campaigns. Three aircraft were deployed to measure physical characteristics and
 110 chemical composition of tropical air masses from the earth's surface up to the stratosphere. In CAST,
 111 the Facility for Airborne Atmospheric Measurements (FAAM) BAe-146 surveyed the boundary
 112 layer and lower troposphere (0-8 km) to sample the convection air mass inflow, while in
 113 CONTRAST the National Science Foundation - National Center for Atmospheric Research (NSF-
 114 NCAR) Gulfstream V (GV) principally targeted the region of maximum convective outflow in the
 115 mid- and upper troposphere, and also sampled down to the boundary layer ~~on occasion~~ (1-14
 116 km). Finally, in ATTREX, the NASA Global Hawk (GH) sampled the TTL (13-20 km) to cover air
 117 masses likely to be detrained from the higher convective outflow. For more details on these
 118 campaigns ~~and the, in particular,~~ objectives, meteorological conditions and descriptions of
 119 individual flights, please refer to the campaign summary papers: Harris et al., 2017 (CAST), Pan et
 120 al., 2017 (CONTRAST) and Jensen et al., 2017 (ATTREX). ATTREX had four active measurement
 121 campaigns, and we also consider the second campaign which was based in Los Angeles in January-
 122 March 2013 and which extensively sampled the East and Central Pacific TTL in six research flights.

123 **2.2 Measurements of the VSL halocarbons**

124 Whole Air Samplers (WAS) were deployed on all three aircraft to measure VSL halocarbons. The
 125 FAAM BAe-146 and NSF-NCAR GV also used on-board gas chromatography-mass spectrometry
 126 (GC-MS) system for real-time analysis (Wang et al., 2015; Andrews et al., 2016; Pan et al., 2017),
 127 though these measurements are not used in our analysis. WAS instrumentation is well established
 128 and has ~~had~~ been used routinely in previous deployments. The sampling and analytical procedures

- Formatted: Font: 12 pt
- Formatted: Font: 12 pt
- Formatted: Subscript
- Formatted: Font: 12 pt
- Formatted: Font: 12 pt
- Formatted: Font: 12 pt
- Formatted: Font: 12 pt
- Formatted: Font: 12 pt

- Formatted: Font: 12 pt
- Formatted: Font: 12 pt
- Formatted: Font: 12 pt
- Formatted: Font: 12 pt
- Formatted: Font: 12 pt

- Formatted: Font: 12 pt

are capable of accessing a wide range of mixing ratios at sufficient precision and the measurements from the three aircraft have been shown to be consistent and comparable (Schauffler et al., 1998; Park et al., 2010; Andrews et al., 2016).

The CAST VSL halocarbon measurements were made using the standard FAAM WAS canisters with 30 second filling time. Up to 64 samples could be collected on each flight and these were analysed in the aircraft hangar, usually within 72 hours after collection. Two litres of sample air were pre-concentrated using a thermal desorption unit (Markes) and analysed with GC-MS (Agilent 7890 GC, 5977 Xtr MSD). Halocarbons were quantified using a NOAA calibration gas standard. The measurement and calibration technique is further described and assessed in Andrews et al. (2013; 2016).

The ATTREX AWAS sampler consisted of 90 canisters, being fully automated and controlled from the ground. Sample collection for the AWAS samples was determined on a real-time basis depending on the flight plan altitude, geographic location, or other relevant real-time measurements. The filling time for each canister ranged from about 25 seconds at 14 km to 90 seconds at 18 km. Canisters were immediately analysed in the field using a high performance GC-MS coupled with a highly sensitive electron capture detector. The limits of detection are compound-dependent and vary from ppt to sub-ppt scale, set at 0.01 ppt for CHBr_3 , CH_2Br_2 and CH_3I (Navarro et al., 2015). A small artefact of $\sim 0.01\text{--}0.02$ ppt for CH_3I cannot be excluded. AWAS samples collected on the GV were analysed with the same equipment. Detailed comparison of measurements from the three systems found agreement within $\sim 7\%$ for CHBr_3 , $\sim 3\%$ for CH_2Br_2 , and 15% for CH_3I (Andrews et al., 2016).

2.3 UK Meteorological Office NAME Lagrangian Particle Dispersion Model

The Lagrangian particle dispersion model, NAME_v (Jones, et al., 2007), is used to simulate the transport of air masses in the Pacific troposphere and the TTL. Back trajectories are calculated with particles being moved through the model atmosphere using operational analyses by mean wind fields (0.352° longitude and 0.235° latitude, i.e. ~ 25 km, with 31 vertical levels below 19 km) calculated by the Meteorological Office's Unified Model at 3-hour intervals (see). This is supplemented by a random walk turbulence scheme to represent dispersion by unresolved aspects of the flow (Davies et al., 2005). For this analysis, the NAME model is used with the improved convection scheme (Meneguz and Thomson, 2014) which simulates displacement of particles subject to convective motions more realistically than previously (Meneguz et al., in review). NAME is run backward in time to determine the origin(s) of air measured at a particular location (WAS sample) along the ATTREX GH flight track.

15,000 particles are released from each point along the flight track where VSL halocarbons were measured in WAS samples. To initialise the NAME model, particles are released randomly in a volume with dimensions $0.1^\circ \times 0.1^\circ \times 0.3$ km centred on each sample. As particles are followed 12 days back in time, trajectories are filtered on the basis of first crossing into the boundary layer (1 km). Subsequently, the fraction of particles which crossed below 1 km is calculated for each WAS measurement point (Ashfold et al., 2012). The NAME 1 km fractions are indicative of the boundary layer air mass influence to the TTL. The 1 km boundary layer fractions are then used to quantitatively estimate the VSL halocarbon contribution to the TTL from the boundary layer, $[\text{X}]_{\text{BL_Contribution}}$. In order to compare the measured and modelled halocarbon values, estimates of the contribution from the background troposphere, $[\text{X}]_{\text{BG_Contribution}}$ (i.e. air which has not come from the

Formatted: Font: 12 pt

Formatted: Font: 12 pt

Formatted: Font: 12 pt

Formatted: Font: 12 pt

Formatted: Font: 12 pt

Formatted: Font: 12 pt

Formatted: Font: 12 pt

Formatted: Font: 12 pt

Formatted: Font: 12 pt

Formatted: Font: 12 pt

Formatted: Font: 12 pt

Formatted: Font: 12 pt

Formatted: Font: 12 pt

Formatted: Font: 12 pt

Formatted: Font: 12 pt

Formatted: Font: 12 pt

Formatted: Font: 12 pt

Formatted: Font: 12 pt

Formatted: Font: 12 pt

Formatted: Font: 12 pt

Formatted: Font: 12 pt

Formatted: Font: 12 pt

Formatted: Font: 12 pt

Formatted: Font: 12 pt

Formatted: Font: 12 pt

Formatted: Font: 12 pt

Formatted: Font: 12 pt

Formatted: Font: 12 pt

Formatted: Font: 12 pt

Formatted: Font: 12 pt

Formatted: Font: 12 pt

Formatted: Font: 12 pt

Formatted: Font: 12 pt

Formatted: Font: 12 pt

Formatted: Font: 12 pt

Formatted: Font: 12 pt

Formatted: Font: 12 pt

Formatted: Font: 12 pt

Formatted: Font: 12 pt

Commented [HN1]: Status??

boundary layer within 12 days) are made. The model estimate for the total halocarbon mixing ratio, $[X]_{NAME_TTL}$, is thus given by Eq. (1):

$$[X]_{NAME_TTL} = [X]_{BL_Contribution} + [X]_{BG_Contribution} \quad (1)$$

The methods for calculating $[X]_{BL_Contribution}$ and $[X]_{BG_Contribution}$ are now described.

2.3.1 NAME modelled boundary layer contribution

The contribution from the boundary layer, ($[X]_{BL_Contribution}$ - described above) to the VSLs in the TTL can be estimated using

- (i) the fractions of trajectories crossing below 1 km in the previous 12 days;
- (ii) the transport times to the TTL calculated for each particle;
- (iii) the initial concentration values for CH_3I , $CHBr_3$ and CH_2Br_2 ; and
- (iv) their atmospheric lifetimes (to account for the photochemical removal along the trajectory).

More specifically, the boundary layer contribution to the TTL for the VSL halocarbons is calculated using Eq. (2) and Eq. (3):

$$[X]_{BL_Contribution,t} = [X]_{BL} \times fraction_t \times \exp(-t/\tau) \quad (2)$$

$$[X]_{BL_Contribution} = \sum([X]_{BL_Contribution,t}) \quad (3)$$

Equation (2) gives the boundary layer contribution to the TTL for a given tracer, X (where X could be CH_3I , $CHBr_3$, CH_2Br_2), at model output time step, t. The model output time step used is 6 hours, from t = 0 (particle release) to t = 48 (end of a 12 day run). $[X]_{BL}$ stands for the initial boundary layer concentration of a given tracer - assigned to each particle which crossed below 1 km (Table 1). $Fraction_t$ is a number of particles which first crossed 1 km in a model output time step, t, over a total number of particles released, and $\exp(-t/\tau)$ is a term for the photochemical loss (where τ stands for atmospheric lifetime of a respective VSL halocarbon). Equation (3) gives the boundary layer contribution that is the sum of boundary layer contribution components in all model output time steps (for t = 1 to 48).

Equation (2) calculates the decay of each tracer after it leaves the boundary layer (0-1 km) which is valid for a well-mixed boundary layer. Since 15,000 particles are released for each AWAS sample, contributions from each particle from below 1 km in the previous 12 days are summed. Decay times, τ , of 4, 15 and 94 days for CH_3I , $CHBr_3$ and CH_2Br_2 , respectively, are used (i.e. constant chemical loss rate) (Carpenter et al., 2014). Thus, a particle getting to the TTL in 1 day contributes more of a given tracer to that air mass than a particle taking 10 days. Once this chemical loss term was taken into account, the NAME trajectories can be used to calculate the contribution of convection of air masses from the boundary layer within the preceding 12 days.

The initial boundary layer concentrations are derived from the CAST and CONTRAST WAS measurements taken in the West Pacific in the same period of January-March 2014 as for the ATTREX measurements in the TTL (Table 1). These observed means are used in model calculations, and the similarity between them and literature values reported in Carpenter et al. (2014) is seen, with lower values for $CHBr_3$ only.

2.3.2 NAME modelled background contribution

To compare our model results against the AWAS observations, the background contribution, $[X]_{BG_Contribution}$ (meaning the contribution from the fraction of trajectories which do not cross below 1 km within 12 days) also needs to be accounted for. This requires estimates for the fraction of trajectories from the free troposphere, which is $(1 - fraction_{BL})$, Eq. (4), and an estimate of the halocarbon mixing ratio in that fraction, $[X]_{BG}$, Eq. (5) i.e.

Formatted: Font: 12 pt

Formatted: Space After: 6 pt

Formatted: Font: 12 pt

Formatted: Font: 12 pt

Formatted: Font: 12 pt

Formatted: Font: 12 pt

Formatted: Font: 12 pt

Formatted: Font: 12 pt

Formatted: Font: 12 pt

Formatted: Font: 12 pt

Formatted: Font: 12 pt

Formatted: Font: 12 pt

Formatted: Font: 12 pt

Formatted: Space After: 6 pt

Formatted: Font: 12 pt

Formatted: Font: 12 pt

Formatted: Font: 12 pt

Formatted: Font: 12 pt

Formatted: Font: 12 pt

Formatted: Font: 12 pt

Formatted: Font: 12 pt

Formatted: Font: 12 pt

Formatted: Font: 12 pt

Formatted: Font: 12 pt

Formatted: Font: 12 pt

Formatted: Font: 12 pt

Formatted: Font: 12 pt

Formatted: Font: 12 pt

Formatted: Font: 12 pt

Formatted: Font: 12 pt

Formatted: Font: 12 pt

Formatted: Font: 12 pt

Formatted: Font: 12 pt

Formatted: Font: 12 pt

Formatted: Font: 12 pt

Formatted: Font: 12 pt

Formatted: Font: 12 pt

Formatted: Font: 12 pt

Formatted: Font: 12 pt

Formatted: Font: 12 pt

$$fraction_{BL} = \sum(fraction_t) \quad (4)$$

$$[X]_{BG_Contribution} = (1 - fraction_{BL}) \times [X]_{BG} \quad (5)$$

Since each sample has 15,000 back-trajectories associated with it, some of which came from below 1 km and some of which did not, a definition as to which air samples are considered as boundary layer and which are considered background is required. Two approaches are tested—~~Both which~~ use the NAME calculations to identify AWAS samples in all flights (2013 and 2014) with low convective influence by (i) filtering for air masses with boundary layer fraction values less than 1, 5 or 10 %; ~~and or~~ (ii) selecting the lowest 10 % of boundary layer fractions. Then, the CH₃I, CHBr₃ and CH₂Br₂ AWAS observations, corresponding to the boundary layer fraction values less than 1, 5 or 10 %, or the lowest 10 % of boundary layer fractions, are averaged to provide CH₃I, CHBr₃ and CH₂Br₂ background mixing ratios. ~~These two~~ approaches are explored below (Sect. 3.1.2).

2.3.3 The effect of assuming constant lifetimes

~~The lifetimes of the halocarbons are not the same in the boundary layer and the TTL (Carpenter et al. 2014). The assumption of constant lifetime in a 12 day trajectory is evaluated by calculating the difference between idealised trajectories which had 2, 4, 6, 8, and 10 days in the boundary layer and 10, 8, 6, 4, and 2 days in the upper troposphere. Lifetimes for the boundary layer and for the upper troposphere for each gas were taken from Carpenter et al. (2014). (Lifetimes for higher altitudes are not available therein). The difference found between the two extreme cases are 6% (CHBr₃), 3% (CH₂Br₂) and 25% (CH₃I). The assumption is thus valid for the two brominated species.~~

~~This assumption is more robust than it might seem at first glance. The boundary layer fraction is calculated using 12 day trajectories in which there is little loss of CH₂Br₂ whether a lifetime of 94 or 150 days is taken. The most important factor in determining the amount lofted into the TTL is thus the original mixing ratio which is only slightly modulated by the chemical loss in 12 days. The longer lifetime is absorbed implicitly, and ~~is not~~ implicitly taken into account in the background contribution. The same arguments apply for CHBr₃, though the effect is a bit larger. The largest difference is seen for CH₃I. However, the difference matters much less for CH₃I because only 4-5% remains after the full 12 days which is much smaller than the uncertainties in this analysis so that much shorter trajectories are used to validate the new convection scheme.~~

3 Analysis of ATTREX 2014 Research Flight 02

We start by showing our results from ~~one of the individual~~ a single ATTREX 2014 ~~Research-research~~ ~~Flights~~ flights, RF02, to illustrate the method. This is followed by analysing all ~~research flights~~ ~~Research Flights~~ together for ATTREX 2014 and 2013 in Sect. 4, and calculating the modelled contribution of active bromine from ~~very short-lived brominated substances~~, CHBr₃ and CH₂Br₂, to the TTL (Sect. 5).

3.1 Individual ATTREX 2014 Flight: Research Flight 02

Figure 1 shows the vertical distribution of CH₃I, CHBr₃ and CH₂Br₂ in the TTL observed during ~~the individual~~ research flight, RF02, during ATTREX 2014. Held on 16-17 February 2014, RF02 was conducted in a confined area east of Guam (12-14° N, 145-147° E) due to a faulty primary satellite communications system for Global Hawk command and control (Jensen, et al., 2017). ~~26- Twenty six~~ vertical profiles through TTL were made, with 86 AWAS measurements taken in total. A high degree of variability of CH₃I in the TTL was observed (from > 0.4 ppt at 14-15 km, to near-zero ppt values at 17-18 km). Each profile, in general, showed a gradation in CH₃I distribution in the TTL. Higher values were measured in the lower TTL up to 16 km, with values decreasing with altitude. The same pattern was observed for CHBr₃ and CH₂Br₂, with the highest concentrations measured in the lower TTL (14-15 km), and the lowest at 17-18 km.

3.1.1 NAME modelled boundary layer contribution

Formatted: Font: 12 pt

Formatted: Font: 12 pt

Formatted: Font: 12 pt

Formatted: Font: 12 pt

Formatted: Font: 12 pt

Formatted: Font: 12 pt

Formatted: Font: 12 pt

Formatted: Font: 12 pt

Formatted: Font: 12 pt

Formatted: Font: 12 pt

Formatted: Font: 12 pt

Formatted: Font: 12 pt

Formatted: Font: 12 pt

Formatted: Font: 12 pt

Formatted: Font: 12 pt

Formatted: Font: 12 pt

Formatted: Font: 12 pt

Formatted: Font: 12 pt

Formatted: Font: 12 pt

Formatted: Font color: Text 1

Formatted: Font color: Text 1, Subscript

Formatted: Font color: Text 1

Formatted: Font color: Text 1, Subscript

Formatted: Font color: Text 1

Formatted: Font color: Text 1, Subscript

Formatted: Font color: Text 1

Formatted: Font color: Text 1, Subscript

Formatted: Font color: Text 1

Formatted: Font color: Text 1, Subscript

Formatted: Font color: Text 1

Formatted: Font color: Red

Formatted: Font: 12 pt

Formatted: Space After: 6 pt

Formatted: Font: 12 pt

Formatted: Font: 12 pt

Formatted: Font: 12 pt

Formatted: Font: 12 pt

Figure 2(a) shows the vertical distribution of the boundary layer air contribution to the TTL (corresponding to the AWAS measurement locations along the RF02 flight track). It reveals higher boundary layer air influence in the lower TTL, decreasing with altitude (similarly to the VSL halocarbon observations). Cumulatively, the highest fractions from below 1 km are found for the lower TTL (14-15 km). A noticeable decrease occurs between the lower and upper TTL (15 to 17 km). From 16 km up, little influence (indicated by <10 % and <5 % 1 km fractions of trajectories below 1 km for 16-17 km and 17-18 km, respectively) of the low-level air masses is seen.

Figure 2(b) shows all NAME runs for RF02 grouped into four 1 km TTL bins: 14-15 km, 15-16 km, 16-17 km and 17-18 km. In the 14-15 km bin, most particles from the low troposphere ~~are calculated to have~~ arrived in the preceding 4 days with many in the preceding 2 days. This represents the fast vertical uplift of the low tropospheric air masses to the lower TTL. At 15-16 km, two particle populations are observed: the first group results from recent vertical uplift, while the second group has been in the upper troposphere for longer than a couple of days (see Fig. 2c in Navarro et al., 2015 for similar example). Above 16 km, the overwhelming majority (>90 %) of the released particles are calculated to be in the TTL for the previous 12 days, with negligible evidence for transport from the low troposphere. This shows the dominance of the long-range, horizontal transport for the 16-17 and 17-18 km NAME runs (also shown in Navarro et al., 2015).

Figure 3 shows the locations at which trajectories crossed 1 km, thereby indicating boundary layer source regions for the RF02 TTL air masses. Boundary layer sources in the ~~W~~western and ~~C~~central Pacific are the most important for the lowest TTL bin (14-15 km, Fig. 3a) in this flight. The Maritime Continent, the Northern Australia coast, the Indian Ocean and the equatorial band of the African continent increase in ~~relative~~ importance as altitude increases, though the overall contribution of recent boundary layer air masses decreases with increasing altitude.

Figure 4 shows the NAME modelled boundary layer contribution to the TTL for CH₃I, CHBr₃ and CH₂Br₂ during RF02. It is important to note that this contribution corresponds to uplift from below 1 km in the preceding 12 days, the length of the trajectories. The calculated boundary layer contributions for CH₃I, CHBr₃ and CH₂Br₂ from the 1 km fractions are highest at 14-15 km, dropping off with altitude. Almost no boundary layer contribution is found for 17-18 km (with values close to 0 ppt).

3.1.2 NAME modelled background contribution

Here we explore the two approaches ~~described~~ summarised in Sect. 2.3.2 for estimating the CHBr₃ and CH₂Br₂ background mixing ratios. Similar values are seen in ATTREX 2013 and 2014. Less variation is observed for CH₂Br₂ due to its longer atmospheric lifetime.

ATTREX 2013 and 2014 are treated separately in the analysis presented below due to the difference in CH₃I background estimates. The approach using the lowest 10 % of the boundary layer fractions is used to estimate the background contribution for the 2014 flights as not enough data meet the former condition due to the proximity of the flights to strong convection. The background values, inferred from all the ATTREX 2014 flights, are used in the individual flight calculations as again there are not enough data from an individual flight to make background calculations for that flight. In ATTREX 2013 we use the boundary layer fractions less than 5 % approach for the CH₃I background estimation. The ATTREX 2014 background estimates should be taken as upper limits as it is hard to identify samples with no convective influence in 2014. This is especially true for the lower TTL since the ATTREX 2014 flights were close to the region of strong convection.

Figure 5 shows the VSL background mixing ratios calculated for the ATTREX campaigns in 2013 and 2014. In ATTREX 2013, low CH₃I background mixing ratios are found. All approaches show similar background mixing ratios. In 2014, higher CH₃I background mixing ratios are calculated due to ubiquity of air from recent, vertical uplift. No boundary layer fractions less than 1 % are found for the 14-17 km bins, and less than 5 % for the 14-15 km.

Formatted: Font: 12 pt

Formatted: Font: 12 pt

3.1.3 NAME modelled total concentrations

The NAME boundary layer and background contribution estimates are added to give an estimate for total halocarbon mixing ratio, $[X]_{\text{NAME_TTL}}$ (Eq. (1)), for comparison with the AWAS observations.

Figure 6 and Table 2 show the vertical distribution of NAME-based estimates for CH_3I , CHBr_3 and CH_2Br_2 in the TTL for RF02. The sums of the NAME CH_3I , CHBr_3 and CH_2Br_2 boundary layer and background contribution estimates agree well with the AWAS observations for all the 1 km TTL bins (compared with Fig. 1).

At 14-15 km, the modelled boundary layer contribution of CH_3I is similar to the observations, indicating recent, rapid convective uplift. This provides evidence that the improved convection scheme provides a realistic representation of particle displacement via deep convection. At higher altitudes, the background contribution is more important and, indeed, the modelled total CH_3I values are greater than the observations. This overestimate of the background contribution results from the difficulty of identifying samples with no convective influence in ATTREX 2014. This problem is most important for CH_3I with its very short lifetime.

CHBr_3 drops off slower with altitude than CH_3I and quicker than CH_2Br_2 . At 14-15 km, the boundary layer contribution accounts for ~ 50 % of the modelled sums of CHBr_3 and CH_2Br_2 , but less than 5 % for CHBr_3 and CH_2Br_2 at 17-18 km. For the upper TTL, the background contribution estimates constitute over 85 % of the modelled sums, thus taking on more importance.

4 The role of transport in the VSL halocarbon distribution in the TTL

The role of transport in the CH_3I , CHBr_3 and CH_2Br_2 distribution in the TTL is examined in this section by applying the NAME based analysis introduced in Sect. 3 to all CH_3I , CHBr_3 and CH_2Br_2 AWAS observations in the ATTREX 2013 and 2014 campaigns.

In ATTREX 2013, six flights surveyed the East Pacific TTL in February-March 2013. Four flights went west from Dryden Flight Research Centre to the area south of Hawaii, reaching 180° longitude. Little influence of convective activity was observed. Most samples with strong boundary layer influence were observed in air masses that had originated over the West Pacific and the Maritime Continent, where it was uplifted to the TTL and transported horizontally within the TTL (Navarro et al., 2015). Two flights sampled the TTL near the Central and South American coast. Few convective episodes were observed. The sampled air had predominantly a small boundary layer air signature from the West Pacific and the Maritime Continent.

In ATTREX 2014, two transit flights and six research flights were made in the West Pacific in January-February 2014. This period coincided with the active phase of Madden-Julian Oscillation (MJO) and increased activity of tropical cyclones. A large influence of recent convective events is observed (Navarro et al., 2015), reflected in the elevated CH_3I and CHBr_3 mixing ratios and the high values of NAME fractions of trajectories below 1 km. All three aircraft flew together in 2014 and so there is a more complete set of measurements from the ground up. Accordingly, this year is discussed first.

4.1 VSL halocarbon distribution in the TTL: ATTREX 2014

Figure 7 shows the vertical distribution of the observations and of the modelled boundary layer contribution and total mixing ratios for CH_3I , CHBr_3 and CH_2Br_2 for all the ATTREX 2014 flights (using only the AWAS measurements made from 20° N southward). As in RF02, CH_3I is highest in the lower TTL, dropping off with altitude. Large flight-to-flight variability in CH_3I measurements is seen. The fraction of NAME particles that travel below 1 km in the previous 12 days (Table 3) are highest at 14-15 km (mean of 57 %) and decrease with altitude in a similar fashion. The CH_3I boundary layer contribution explains most of the observations for the 14-15 and 15-16 km layers. Disparities in observed and modelled CH_3I arise from 16 km up. Estimated background estimate

Formatted: Font: 12 pt

357 values are ~~minimal~~very low, oscillating between 0 and the limit of detection of the AWAS
358 instrument for the iodinated short-lived organic substances, 0.01 ppt. The sums of the CH₃I boundary
359 layer and background contribution estimates show good agreement with AWAS observations for all
360 the TTL 1 km segments (Table 3).

Formatted: Font: 12 pt

361 The good agreement for the 14-15 km and 15-16 km layers can be attributed to the improved
362 representation of deep convection in NAME, provided by the new convection scheme (Meneguz et
363 al., in review). However, there is an underestimation of the boundary layer contribution to the upper
364 TTL levels (16-17 and 17-18 km) which we attribute to the new convection scheme not working as
365 well at these altitudes. This is consistent with a known tendency of the Unified Model to
366 underestimate the depth of deepest convection in the tropics (Walters, et al., 2019). Both the CH₃I
367 AWAS observations and the modelled sums are higher than reported previously in the literature
368 (Carpenter et al., 2014) for all the TTL segments. This may be explained by sampling the TTL in a
369 region of high convective activity. This result gives confidence in the quality of the new convection
370 scheme and hence in similar calculations of convective influence on the longer-lived CHBr₃ and
371 CH₂Br₂.

Formatted: Font: 12 pt

372 The highest CHBr₃ and CH₂Br₂ concentrations were observed in the lower TTL (14-15 km),
373 dropping off more slowly with altitude than CH₃I. The weight of the modelled boundary layer
374 contribution estimates to the modelled total amounts varies from approximately 50% at 14-15 km
375 (unlike for CH₃I where over 85 % of the modelled sum is attributed to the boundary layer
376 contribution at 14-15 km) to < 20% at 17-18 km. The sums of the modelled boundary layer and
377 background contributions ~~are in show~~ good agreement with the CHBr₃ and CH₂Br₂
378 AWAS observations. The ATTREX observations and the NAME modelled sums are within the
379 range of values reported in the literature (Carpenter, et al., 2014).

Formatted: Font: 12 pt

Formatted: Font: 12 pt

Formatted: Font: 12 pt

Formatted: Font: 12 pt

380 4.2 VSL halocarbon distribution in the TTL: ATTREX 2013

381 Figure 8 shows the vertical distribution for CH₃I, CHBr₃ and CH₂Br₂ in the TTL, observed and
382 modelled from the ATTREX 2013 flights. Only (using only the AWAS measurements taken south
383 of 20°N are used). Much lower CH₃I values are found in 2013 than in 2014 (Fig. 7). The NAME 1
384 km fractions are considerably lower (~fourfold), and the corresponding CH₃I boundary layer
385 contribution shows values close to the limit of detection of the AWAS instrument for CH₃I. The
386 background contribution comprises over 85-90 % of the sums of the modelled CH₃I estimate in the
387 TTL. Good agreement is found between the AWAS observations and the sums of the modelled
388 boundary layer and background contributions, ~~against the AWAS observations.~~ Both the
389 observed and modelled values are in the low end of the CH₃I concentrations reported by the WMO
390 2014 Ozone Assessment (Carpenter et al., 2014).

Formatted: Font: 12 pt

Formatted: Font: 12 pt

Formatted: Font: 12 pt

Formatted: Font: 12 pt

Formatted: Font: 12 pt

Formatted: Font: 12 pt

391 The ATTREX 2013 mixing ratios are ~~also~~ lower for CHBr₃ and higher CH₂Br₂ than shown in Fig. 7
392 for 2014. The NAME calculated CHBr₃ and CH₂Br₂ boundary layer contributions are small,
393 constituting approximately 10 % of the NAME modelled sums for 14-15 km, and less for the upper
394 TTL segments. The background contribution estimates comprise over 85 % of the modelled sums.
395 Good agreement is found between the sums of the modelled boundary layer and background
396 contributions estimates and the CHBr₃ and CH₂Br₂ AWAS observations.

Formatted: Font: 12 pt

Formatted: Font: 12 pt

397 4.3 ATTREX 2013 and 2014: Inter-campaign comparison

398 Clear differences in the vertical distributions of CH₃I in the TTL are found in ATTREX 2013 and
399 2014. CH₃I estimates, corresponding to high values in the NAME modelled 1 km fractions, are high
400 in 2014, whereas in 2013 almost no CH₃I is estimated to be in the TTL. This is due to the minimal
401 contribution of the boundary layer air within the previous 12 days: ATTREX 2013 was in the East
402 Pacific away from the main region of strong convection. Longer transport timescales result from
403 horizontal transport and were more important in ATTREX 2013, with much less recent convective

influence than in ATTREX 2014. More chemical removal of CH₃I and CHBr₃ thus took place, leading to lower concentrations in the East Pacific TTL.

The trajectories are analysed to investigate the timescales for vertical transport by calculating how long it took particles to go from below 1 km to the TTL. In 2013, almost no episodes of recent rapid vertical uplift are found, with most particles taking 8 days and more to cross the 1 km. This is indicative of the dominant role of long-range horizontal transport. In 2014, by way of contrast, a considerable number of trajectories (10's of per cent) come from below 1 km in less than 4 days, representing the 'young' air masses being brought from the low troposphere via recent and rapid vertical uplift.

The spatial variability in the boundary layer ~~air source origins~~ mixing ratios corresponding to different source strengths coupled well, as well as the variation in atmospheric transport pathways and transport timescales can explain the differences in the distribution of the NAME 1 km fractions in the TTL. In 2014 (2013), higher (lower) boundary layer fractions corresponded well with higher (lower) CH₃I and CHBr₃ values in the TTL, especially with the highest concentrations occurring for the flights with the most convective influence and the highest fractions of particles arriving within the 4 days.

In ~~the ATTREX 2014 flights~~, the western and central Pacific is the dominant source origin of boundary layer air to the TTL (Navarro et al., 2015). Increased tropical cyclone activity in this area (particularly Faxai 28 February – 6 March 2014 and Lusi 7-17 March 2014) and the strong signal from the Madden Julian Oscillation (MJO - an intraseasonal phenomenon characterised by an eastward spread of large regions of enhanced and suppressed tropical rainfall, mainly observed over the Indian and Pacific Ocean), ~~MJO~~-related convection contributed to the more frequent episodes of strong and rapid vertical uplifts of the low-level air to the TTL. A significant contribution is also seen from the central Indian Ocean, marking the activity of the Fobane tropical cyclone (6-14 February 2014). Minimal contribution from the other remote sources (Indian Ocean, African continental tropical band) is found (Anderson et al., 2016; Jensen et al., 2017; Newton et al., 2018).

5 How much do VSL bromocarbons contribute to the bromine budget in the TTL?

The NAME modelled CHBr₃ and CH₂Br₂ estimates in the TTL are used to calculate how much bromine from the VSL bromocarbons, Br-VSL_{org}, is found in the lower stratosphere, based on how much enters the TTL in the form of bromocarbons (~~as in~~ Navarro et al. (2015)). CHBr₃ and CH₂Br₂ are the dominant short-lived organic bromocarbons, and the minor bromocarbons: CH₂BrCl, CHBr₂Cl and CHBrCl₂ are excluded here (~~as~~ their combined contribution is less than 1 ppt to Br-VSL_{org} at 14-18 km, Navarro et al., 2015). The NAME modelled CHBr₃ and CH₂Br₂ estimates are multiplied by the number of bromine atoms (bromine atomicity), and then summed to yield the total of Br-VSL_{org}.

Figure 9 shows the contribution of CHBr₃ and CH₂Br₂, the two major VSL bromocarbons contributing to the bromine budget in the TTL. For ATTREX 2013 and 2014, similar contributions of CHBr₃ and CH₂Br₂ to Br-VSL_{org} are found in the lower TTL. In 2014, CHBr₃ in the lower TTL was abundant enough to contribute as much Br-VSL_{org} as CH₂Br₂. A combination of larger boundary layer air influence in the TTL and shorter mean transport times to reach the TTL result in the observed higher CHBr₃ contribution to the Br-VSL_{org} in the lower TTL in 2014, than in 2013. The CH₂Br₂ contribution dominates in the upper TTL due to its longer atmospheric lifetime.

Good agreement is found between the bromine loading from the VSL bromocarbons, inferred from the NAME modelled estimates initialised with BAe-146 and GV measurements, and the Global Hawk AWAS observations. Higher organic bromine loading is seen around the cold point tropopause (16-17 km) in ATTREX 2014.

Using the upper troposphere measurements taken during the SHIVA campaign in the western Pacific in November-December 2011, Sala et al. (2014) calculated an estimate for VSLS (CHBr₃, CH₂Br₂,

Formatted: Font: 12 pt

Formatted: Font: 12 pt

Formatted: Font: 12 pt

Formatted: Font: 12 pt

CHBrCl₂, CH₂BrCl, CHBr₂Cl) contribution to the organic bromine at the level of zero radiative heating (15.0 - 15.6 km). Air masses reaching this level are expected to reach the stratosphere. This VLS mean mixing ratio estimate of 2.88 (+/- 0.29) ppt (2.35 ppt for CHBr₃ and CH₂Br₂, excluding minor short-lived bromocarbons) is lower due to a lower contribution from CHBr₃ estimate (0.22 ppt compared to the CHBr₃ estimate for NAME / ATTREX in Table 5). Compared to other literature values reported in Sala et al., (2014), Our estimates of the contribution of CHBr₃ and CH₂Br₂ to the organic bromine at the LZRH are slightly higher largely than those in Sala et al. (2014) due to a higher estimate for a shorter-lived CHBr₃.

Several papers use the same measurements from the combined ATTREX/CAST/CONTRAST campaign in 2014 and from the other ATTREX phases. Navarro et al. (2015) report slightly higher bromine loading from the Br-VSL_{org} at the tropopause level (17 km) in the West Pacific, 2014 than in the East Pacific, 2013 (the Br-VSL_{org} values from the AWAS observations were of 3.27 (+/-0.47) and 2.96 (+/-0.42) ppt, respectively). The minor short-lived organic bromine substances were included in the analysis of Navarro et al. (2015), accounting for the higher Br-VSL_{org}. Butler et al. (2017, 2018), report a mean mole fraction and range of 0.46 (0.13-0.72) ppt and 0.88 (0.71-1.01) ppt of CHBr₃ and CH₂Br₂ being transported to the TTL during January and February 2014. This is consistent with a contribution of 3.14 (1.81-4.18) ppt of organic bromine to the TTL over the region of the campaign. The most recent study on stratospheric analysis of the injection of brominated VLS into the TTL by Wales et al. (2018), using the CAM-chem-SD model combined with a steady state photochemical box model has shown, using different methodology and CONTRAST and ATTREX data found that 2.9 +/- 0.6 ppt of bromine enters the stratosphere via organic source gas injection of VLS. The NAME modelled results presented here (Fig. 9, Table 5) are thus in good agreement with the values reported by Navarro et al. (2015), Butler et al. (2017, 2018) and Wales et al. (2018).

The NAME modelled results presented here (Fig. 9, Table 5) are in good agreement with the values reported by Navarro et al. (2015) and Butler et al. (2017).

6 Summary and Discussion

We have used the NAME trajectory model in backward mode to assess the contribution of recent convection to the mixing ratios of three short-lived halocarbons, CH₃I, CHBr₃ and CH₂Br₂. 15,000 back-trajectories are computed for each measurement made with the whole air samples on the NASA Global Hawk in ATTREX 2013 and 2014, and the fraction that originated below 1 km is calculated for each sample. A steep drop-off in this fraction is observed between 14-15 km and 17-18 km. Low level measurements of CH₃I, CHBr₃ and CH₂Br₂ from the FAAM BAe-146 and the NCAR GV are used in conjunction with these trajectories and an assumed photochemical decay time to provide estimates of the amount of each gas reaching the TTL from below 1 km. Comparison of these modelled estimates with the CH₃I measurements shows good agreement with the observations at the lower altitudes in the TTL values, with less good agreement at altitudes > 16 km, though it should be noted that the amounts are very small here. The lifetime of CH₃I is 3-5 days, and so there is a > 90 % decay in the 12 day trajectories. The comparison between the modelled and measured CH₃I thus indicates that the NAME convection scheme is realistic up to the lower TTL but less good at reproducing the small number of extreme convective events that penetrate to the upper TTL.

In order to perform similar calculations for the longer-lived bromocarbons, an estimate of the background free tropospheric concentration is required. This is calculated found by considering bromocarbon values in samples where there was only a small influence from the boundary layer, i.e. where very few NAME trajectories passed below 1 km. This is possible in 2013 when the ATTREX flights were away from the region of strong convection, but much harder in 2014 when (as planned)

Formatted: Font: 12 pt

Formatted: Font: 12 pt

Formatted: Font: 12 pt

Formatted: Font: 12 pt

Formatted: Font: 12 pt

Formatted: Font: 12 pt

Formatted: Font: 12 pt

Formatted: Font: 12 pt

Formatted: Font: 12 pt

Formatted: Font: 12 pt

Formatted: Font: 12 pt

Formatted: Font: 12 pt

Formatted: Font: 12 pt

Formatted: Font: 12 pt

Formatted: Font: 12 pt

Formatted: Font: 12 pt, Font color: Text 1

Formatted: Font color: Text 1

Formatted: Font: 12 pt, Font color: Text 1

Formatted: Font color: Text 1

Formatted: Font: 12 pt

Formatted: Space After: 6 pt

Formatted: Space After: 10 pt, Line spacing: Multiple 1.15 li

Formatted: Space After: 6 pt

Formatted: Font: 12 pt

Formatted: Font: 12 pt

Formatted: Font: 12 pt

Formatted: Font: 12 pt

the flights were heavily influenced by convection. By summing the boundary layer and background contributions, an estimate of the total bromocarbon mixing ratio is obtained.

The resulting modelled estimates are found to be in generally good agreement with the ATTREX measurements. In other words, a high degree of consistency is found between the low altitude halocarbon measurements made on the BAe-146 and GV and the high altitude measurements made on the Global Hawk when they are connected using trajectories calculated by the NAME dispersion model with its updated convection scheme and driven by meteorological analyses with 25 km horizontal resolution. There are some indications of the modelled convection not always reaching quite high enough, but this is consistent with a known tendency of the Unified Model to underestimate the depth of the deepest convection in the tropics.

The resolved winds are likely to be well represented, at least partly because the wind data is analysis rather than forecast data. Hence we expect the main errors in the modelling to arise from the representation of convection. Individual convective events are hard to model and can have significant errors. However because the upper troposphere concentrations depend on a number of convective events and we are considering a range of flights and measurements locations, our conclusions on general behaviour should be robust. The consistency between the aircraft measurements and the NAME simulations supports this.

In the above, the boundary layer contribution arises from trajectories which visit the boundary layer within 12 days while the background contribution involves air that has been transported into the TTL from outside the boundary layer on timescales up to 12 days. Sensitivity tests were performed in which the trajectories were followed for longer than 12 days: the effect was to re-allocate some of the air from the background category into the boundary layer contribution with no net change in the total.

The approach using NAME trajectories and boundary layer measurements produces Br-VSL_{org} estimates of 3.47-5.2 +/- 0.4 (3.3 +/- 0.4) ppt in the lower East (West) Pacific TTL (14-15 km) and 2.5 +/- 0.2 (2.4 +/- 0.4) ppt in the upper East (West) Pacific TTL (17-18 km). These lie well within the range of the recent literature findings (Tegtmeier et al., 2012; Carpenter et al., 2014; Liang et al., 2014; Navarro et al., 2015; Butler et al., 2017; [Wales et al. 2018](#)). The validation with the ATTREX measurements provides confidence that a similar approach could be used for years when high altitude measurements are not available assuming that realistic estimates of the background tropospheric contributions can be obtained from either models or measurements.

Our study of boundary layer contribution of bromoform and dibromomethane into the TTL in the West Pacific, using a combined approach of NAME Lagrangian dispersion modelling and CAST, CONTRAST and ATTREX 2014 measurements, has successfully validated an improved updated convection scheme for use with the NAME trajectory model. The previous parameterisation scheme was reasonable for convection at mid-latitudes but was far too weak to represent the stronger tropical convection. Comparison with the extensive CH₃I measurements made in this campaign provides good support for its use in modelling transport in tropical convective systems. (New scheme: <https://www.harmonia.org/conferences/proceedings/Madrid/publishedSections/H15-29.pdf> - please note the full paper is accessible upon request – contact Dr David Thomson from the UK Met Office, Atmospheric Dispersion and Air Quality Unit).

This represents a considerable improvement. As the old convective scheme was used in the earlier study by Ashfold et al. (2012) which used the old convection scheme and using the East Pacific measurements, this represents a considerable improvement which found reasonable agreement up to and including the level of maximum convective outflow, but not above, when compared to measurements in the East Pacific from CR-AVE and TC4. The approach used by Ashfold et al. (2012) was to use the NAME dispersion model with its updated convection scheme and driven by meteorological analyses with 25 km horizontal resolution. There are some indications of the modelled convection not always reaching quite high enough, but this is consistent with a known tendency of the Unified Model to underestimate the depth of the deepest convection in the tropics.

Formatted: Font: 12 pt

Formatted: Font: 12 pt

Formatted: Font: 12 pt

Formatted: Font: 12 pt

Formatted: Font: 12 pt

Formatted: Font: 12 pt

Formatted: Font: 12 pt

Formatted: Font: 12 pt

Formatted: Font: 12 pt

Formatted: Font: 12 pt

Formatted: Font: Font color: Text 1

Formatted: Space After: 8 pt, Line spacing: Multiple 1.08 li

Formatted: Font: Font color: Text 1, Subscript

Formatted: Font: Font color: Text 1

Formatted: Font: Italic, Underline, Font color: Text 1

Formatted: Font: Italic, Font color: Text 1

Formatted: Font color: Text 1

Formatted: Font: (Default) Times New Roman, 12 pt, Not Italic, Font color: Text 1, Not Highlight

Formatted: Font: Font color: Text 1

Formatted: Font: (Default) Times New Roman, 12 pt, Not Italic, Font color: Text 1, Not Highlight

Formatted: Font: Not Italic, Font color: Text 1

Formatted: Font color: Text 1

Formatted: Font: (Default) Times New Roman, 12 pt, Font color: Text 1, Not Highlight

Formatted: Font: Font color: Text 1

2012), has been further extended so that VSLS mixing ratios can be assigned to contributions from the boundary layer and from the ‘background’ TTL.

Different studies focussed on transport up to the level of maximum convective outflow, including the ones where FLEXPART chemistry-transport model is applied, during the SHIVA campaign based in Malaysian Borneo. The surface concentrations and strength of convection over the South China Sea are different to those over the West Pacific in January–March (winter). Another more recent study by Wales et al., 2018 is based on the Eulerian 3D CAM-chem SD model while this study is based purely on a trajectory-based approach. The agreement between these two studies is good.

Even though this methodology has been applied to many VSLS transport studies before and is a common procedure in the research community, we investigate the VSLS transport from the boundary layer to the stratosphere, comparing it with a new multi-aircraft campaign [below but better phrased], and a further developed model version of NAME with improved convection scheme. It is one of the first studies in which we have combined atmospheric measurements of the entire troposphere and lower stratosphere in the West Pacific region in 2014, and the UK NAME Lagrangian particle dispersion model with improved parameterisation scheme for simulating displacement of particles due to convective motions, to quantify mixing ratios for CH₃I, CHBr₃ and CH₂Br₂ and their estimated contributions from the boundary layer and the background. Firstly, our methodology for quantifying mixing ratios of CH₃I works well as modelled estimates were in good agreement with ATTREX measurements in the TTL. This study also showed that the boundary layer air is the sole source of CH₃I in the upper troposphere, lower stratosphere in the region of deep and frequent convective activity. A bespoke good agreement between modelled and measured CH₃I mixing ratios in the upper troposphere and the TTL makes us confident about the good performance of the improved parameterisation scheme for displacement of particles as a result of deep convection. This methodology, with validated convection scheme for CH₃I, was further applied to quantify mixing ratios of CHBr₃ and CH₂Br₂ in the TTL. As these compounds are longer lived than CH₃I, the boundary layer contribution estimates tend to have less role, with the challenge of estimating the background contribution estimate in a confident manner. The agreement between modelled and measured CHBr₃ mixing ratios was good, and for CH₂Br₂ satisfactory, and for both within the reported literature values. We are confident that our methodology for quantifying boundary layer contribution of CH₃I, CHBr₃ and CH₂Br₂ gives good agreement with measured data, and slightly less confident on the estimates of background contribution, particularly for CH₂Br₂. We would like to further test our methodology by applying it to quantify modelled mixing ratios of short-lived bromocarbons and iodocarbons for any future campaigns that feature source-receptor measurements being taken at the same time and region.

7 Data availability

Formatted

Formatted: Font color: Red

Formatted: Space After: 8 pt, Line spacing: Multiple 1.08 li

Formatted: Font: 12 pt

Formatted: Space After: 6 pt

Formatted: Font: 12 pt

Formatted: Font: 12 pt

Formatted: Font: 12 pt

Formatted: Font: 12 pt

Formatted: Font: 12 pt

Formatted

Formatted: Font: 12 pt

Formatted: Font: 12 pt

Formatted: Font: 12 pt

Formatted

Formatted: Font: 12 pt

Formatted: Font: 12 pt

Formatted: Font: 12 pt

Formatted

Formatted: Font: 12 pt

Formatted: Font: 12 pt

Formatted: Font: 12 pt

Formatted: Font: 12 pt

Formatted

Formatted: Font: 12 pt

Formatted: Font: 12 pt

Formatted: Font: 11 pt, Font color: Red

Formatted: Space After: 8 pt, Line spacing: Multiple 1.08 li

Formatted: Font: (Default) Calibri, 11 pt, Font color: Red

Formatted: Space After: 6 pt

Formatted: Font: 12 pt

Formatted: Space After: 6 pt

588 The CH₃I, CHBr₃ and CH₂Br₂ AWAS data from the NASA ATTREX measurements are available
 589 online in the NASA ATTREX database (<https://espoarchive.nasa.gov/archive/browse/attrex>). The
 590 CAST measurements are stored on the British Atmospheric Data Centre, which is part of the Centre
 591 for Environmental Data archive at
 592 <http://catalogue.ceda.ac.uk/uuid/565b6bb5a0535b438ad2fae4c852e1b3>. The CONTRAST AWAS
 593 data are available through <http://catalog.eol.ucar.edu/contrast>. The NAME data are available from
 594 the corresponding author upon request.

595

596 **8 Author Contribution**

597 The main part of the analysis was conducted by MF. EA and MN provided CH₃I, CHBr₃ and CH₂Br₂
 598 AWAS measurements from the ATTREX and CONTRAST research flights. SA and LC provided
 599 CH₃I, CHBr₃ and CH₂Br₂ measurements from the CAST campaign. MA designed initial scripts for
 600 NAME runs and products. EM and DT developed the model code for improved convection scheme.
 601 MF and NH prepared the manuscript with contributions from all co-authors, NH also supervised this
 602 PhD work.

603

604 **9 Acknowledgements**

605 The authors would like to thank our NASA ATTREX, NCAR CONTRAST and NERC CAST
 606 project partners and the technical teams. MF would like to thank Drs Michelle Cain, Alex Archibald,
 607 Sarah Connors, Maria Russo and Paul Griffiths for their input on the NAME applications for flight
 608 planning and post-flight modelling. The research was funded through the UK Natural Environment
 609 Research Council CAST project (NE/J006246/1 and NE/J00619X/1), and MF was supported by a
 610 NERC PhD studentship. EA acknowledges support from NASA grants NNX17AE43G,
 611 NNX13AH20G and NNX10AOB3A. We acknowledge use of the NAME atmospheric dispersion
 612 model and associated NWP meteorological datasets made available to us by the UK Met Office.

613

614 **10 References**

615 Anderson, D.C., Nicely, J.M., Salawitch, R.J., Canty, T.P., Dickerson, R.R., Hanisco, T.F., Wolfe,
 616 G.M., Apel, E.C., Atlas, E., Bannan, T., Bauguitte, S., Blake, N.J., Bresch, J.F., Campos, T.L.,
 617 Carpenter, L.J., Cohen, M.D., Evans, M., Fernandez, R.P., Kahn, B.H., Kinnison, D.E., Hall, S.R.,
 618 Harris, N.R.P., Hornbrook, R.S., Lamarque, J-F., Le Breton, M., Lee, J.D., Percival, C., Pfister, L.,
 619 Bradley Pierce, R., Riemer, D.D., Saiz-Lopez, A., Stunder, B.J.B., Thompson, A.M., Ullmann, K.,
 620 Vaughan, A., and Weinheimer, A.J.: A pervasive role for biomass burning in tropical high ozone /
 621 low water structures, *Nature Comms*, 7, doi: 10.1038/ncomms10267, 2016.
 622 Andrews, S.J., Jones, C.E., and Carpenter, L.J.: Aircraft measurements of very short-lived
 623 halocarbons over the tropical Atlantic Ocean, *Geophys Res Lett.*, 40 (5), 1005-1010, doi:
 624 10.1002/grl.50141, 2013.
 625 Andrews, S.J., Carpenter, L.J., Apel, E.C., Atlas, E., Donets, V., Hopkins, J.R., Hornbrook, R.S.,
 626 Lewis, A.C., Lidster, R. T., Lueb, R., Minaeian, J., Navarro, M., Punjabi, S., Riemer, D., and
 627 Schauffler, S.: A comparison of very short lived halocarbon (VSLs) and DMS aircraft measurements
 628 in the tropical west Pacific from CAST, ATTREX and CONTRAST, *Atmos. Meas. Tech.*, 9, 5213-
 629 5225, doi: 10.5194/amt-9-5213-2016, 2016.
 630 Ashfold, M.J., Harris, N.R.P., Atlas, E.L., Manning, A.J., and Pyle, J.A.: Transport of short-lived
 631 species into the Tropical Tropopause Layer, *Atmos. Chem. Phys.*, 12, 6309-6322, doi: 10.5194/acp-
 632 12-6309-2012, 2012.

Formatted: Font: 12 pt

Formatted: Space After: 6 pt

Formatted: Font: 12 pt

Formatted: Space After: 6 pt

Formatted: Font: 12 pt

Formatted: Space After: 6 pt

Formatted: Font: 11 pt

Formatted: Space After: 3 pt

Formatted: Font: 12 pt

633 Ball, W.T., Alsing, J., Mortlock, D.J., Rozanov, E.V., Tummon, F., and Haigh, J.D.: Reconciling
634 differences in stratospheric ozone composites, *Atmos. Chem. Phys.*, 17, 12269-12302, doi:
635 10.5194/acp-17-12269-2017, 2017.

636 Ball, W. T., Alsing, J., Staehelin, J., Davis, S. M., Froidevaux, L., and Peter, T.: Stratospheric ozone
637 trends for 1985–2018: sensitivity to recent large variability, *Atmos. Chem. Phys. Discuss.*,
638 <https://doi.org/10.5194/acp-2019-243>, in review, 2019.

639 Butler, R., Palmer, P.I., Feng, L., Andrews, S.J., Atlas, E.L., Carpenter, L.J., Donets, V., Harris,
640 N.R.P., Montzka, S.A., Pan, L.L., Salawitch, R.J., and Schauffler, S.M.: Quantifying the vertical
641 transport of CHBr₃ and CH₂Br₂ over the Western Pacific, *Atmos. Chem. Phys. Discuss.*, doi:
642 10.5194/acp-2016-936, 2016.

643 Carpenter, L. J., Sturges, W. T., Penkett, S. A., Liss, P. S., Alicke, B., Hebestreit, K., and Platt, U.,
644 Short-lived alkyl iodides and bromides at Mace Head, Ireland: Links to biogenic sources and halogen
645 oxide production, *J. Geophys. Res.*, 104, 1679, 1999.

646 Carpenter, L.J., Archer, S.D., and Beale, R.: Ocean-atmosphere trace gas exchange, *Chem. Soc.*
647 *Rev.*, 41 (19), 6473-6506, doi: 10.1039/c2cs35121h, 2012.

648 Carpenter, L.J., Reimann, S., Burkholder, J.B., Clerbaux, C., Hall, B.D., Hossaini, R., Laube, J.C.,
649 and Yvon-Lewis, S.A.: Ozone-depleting substances (ODSs) and other gases of interest to the
650 Montreal Protocol, Chap.1, in *Scientific Assessment of Ozone Depletion, 2014; Global Ozone*
651 *Research and Monitoring Project – Report no 55*, World Meteorological Organisation, Geneva,
652 Switzerland, 2014.

653 Chipperfield, M.P., Bekki, S., Dhomse, S., Harris, N.R.P., Hassler, B., Hossaini, R., Steinbrecht, W.,
654 Thieblemont, R., and Weber, M.: Detecting recovery of the stratospheric ozone layer, *Nature*, 549,
655 211–218, doi: 10.1038/nature23681, 2017.

656 Davies, T., Cullen, M.J.P., Malcolm, A.J., Mawson, M.H., Staniforth, A., White, A.A., and Wood,
657 N.: A new dynamical core for the Met Office’s global and regional modelling of the atmosphere, *Q.*
658 *J. Roy. Meteorol. Soc.*, 131, 1759–1782, doi: 10.1256/qj.04.101, 2005.

659 Dessens, O., Zeng, G., Warwick, N., and Pyle, J.: Short-lived bromine compounds in the lower
660 stratosphere; impact of climate change on ozone, *Atmos. Sci. Lett.*, 10, 201-206, doi:
661 10.1002/asl.236, 2009.

662 Engel, A. and M. Rigby (Lead Authors), J.B. Burkholder, R.P. Fernandez, L. Froidevaux, B.D. Hall,
663 R. Hossaini, T. Saito, M.K. Vollmer, and B. Yao, Update on Ozone-Depleting Substances (ODSs)
664 and Other Gases of Interest to the Montreal Protocol, Chapter 1 in *Scientific Assessment of Ozone*
665 *Depletion: 2018, Global Ozone Research and Monitoring Project–Report No. 58, World*
666 *Meteorological Organization, Geneva, Switzerland, 2018.*

667 Fernandez, R.P., Salawitch, R.J., Kinnison, D.E., Lamarque, J-F., and Saiz-Lopez, A.: Bromine
668 partitioning in the tropical tropopause layer: Implications for stratospheric injection, *Atmos. Chem.*
669 *Phys.*, 14, 13391-13410, doi: 10.5194/acp-14-13391-2014, 2014.

670 Fiehn, A., Quack, B., Hepach, H., Fuhlbrügge, S., Tegtmeier, S., Toohey, M., Atlas, E., and Krüger,
671 K.: Delivery of halogenated very short-lived substances from the west Indian Ocean to the
672 stratosphere during the Asian summer monsoon, *Atmos. Chem. Phys.*, 17, 6723-6741,
673 doi:10.5194/acp-17-6723-2017, 2017.

674 Fueglistaler, S., Dessler, A.E., Dunkerton, T.J., Folkins, I., Fu, Q., and Mote, P.W.: Tropical
675 tropopause layer, *Reviews of Geophysics*, 47 (1), doi:10.1029/2008RG000267, 2009.

676 Fuhlbrügge, S., Quack, B., Tegtmeier, S., Atlas, E., Hepach, H., Shi, Q., Raimund, S., and Krüger,
677 K.: The contribution of oceanic halocarbons to marine and free tropospheric air over the tropical
678 West Pacific, *Atmos. Chem. Phys.*, 16, 7569-7585, doi:10.5194/acp-16-7569-2016, 2016.

679 Harris, N.R.P., Hassler, B., Tummon, F., Bodeker, G.E., Hubert, D., Petropavlovskikh, I.,

Formatted: Font: 12 pt, Font color: Text 1

Formatted: Font: Times New Roman, 12 pt, Font color: Text 1

Formatted: Space After: 3 pt

Formatted: Font: Times New Roman, 12 pt

Formatted: Font: 12 pt

Formatted: Default Paragraph Font, Font: (Default) Times New Roman, 12 pt, Font color: Text 1

Formatted: Font: (Default) Times New Roman, 12 pt, Font color: Text 1

Formatted: Default Paragraph Font, Font: (Default) Times New Roman, 12 pt, Font color: Text 1

Formatted: Font: (Default) Times New Roman, 12 pt, Font color: Text 1

Formatted: Default Paragraph Font, Font: (Default) Times New Roman, 12 pt, Font color: Text 1

Formatted: Font: (Default) Times New Roman, 12 pt, Font color: Text 1

Formatted: Default Paragraph Font, Font: (Default) Times New Roman, 12 pt, Font color: Text 1

Formatted: Font: (Default) Times New Roman, 12 pt, Font color: Text 1

Formatted: Default Paragraph Font, Font: (Default) Times New Roman, 12 pt, Font color: Text 1

Formatted: Font: (Default) Times New Roman, 12 pt, Font color: Text 1

Formatted: Default Paragraph Font, Font: (Default) Times New Roman, 12 pt, Font color: Text 1

Formatted: Font: (Default) Times New Roman, 12 pt, Font color: Text 1

Formatted: Font: (Default) Times New Roman, 12 pt, Not Bold, Font color: Text 1

Formatted: Font: (Default) Times New Roman, 12 pt, Not Bold, Font color: Text 1

Formatted: Font: 12 pt, Font color: Text 1

Formatted: Font: 12 pt

Formatted: Space After: 3 pt

Formatted: Space After: 0.6 line

Formatted: Font: Times New Roman, 12 pt, Font color: Text 1

Formatted: Normal (Web), Space After: 0.6 line, Pattern: Clear (White)

Formatted: Font: 12 pt, Font color: Text 1

Formatted: Font: 12 pt

Formatted: Space After: 0.6 line

Formatted: Space After: 3 pt

Steinbrecht, W., Anderson, J., Bhartia, P.K., Boone, C.D., Bourassa, A., Davis, S.M., Degenstein, D., Delcloo, A., Frith, S.M., Froidevaux, L., Godin-Beekmann, S., Jones, N., Kurylo, M.J., Kyrölä, E., Laine, M., Leblanc, S.T., Lambert, J.-C., Liley, B., Mahieu, E., Maycock, A., de Mazière, M., Parrish, A., Querel, R., Rosenlof, K.H., Roth, C., Sioris, C., Staehelin, J., Stolarski, R.S., Stübi, R., Tamminen, J., Vigouroux, C., Walker, K.A., Wang, H.J., Wild, J., and Zawodny, J.M.: Past changes in the vertical distribution of ozone – Part 3: Analysis and interpretation of trends, *Atmos. Chem. Phys.*, 15, 9965–9982, doi:10.5194/acp-15-9965-2015, 2015.

Harris, N.R.P., Carpenter, L.J., Lee, J.D., Vaughan, G., Filus, M.T., Jones, R.L., OuYang, B., Pyle, J.A., Robinson, A.D., Andrews, S.J., Lewis, A.C., Minaeian, J., Vaughan, A., Dorsey, J.R., Gallagher, M.W., Le Breton, M., Newton, R., Percival, C.J., Ricketts, H.M.A., Bauguitté, S.J.-B., Nott, G.J., Wellpott, A., Ashfold, M.J., Flemming, J., Butler, R., Palmer, P.I., Kaye, P.H., Stopford, C., Chemel, C., Boesch, H., Humpage, N., Vick, A., MacKenzie, A.R., Hyde, R., Angelov, P., Meneguz, E., and Manning, A.J.: 2017: Coordinated Airborne Studies in the Tropics (CAST), *Bull. Amer. Meteor. Soc.*, 98, 145–162, doi: 10.1175/BAMS-D-14-00290.1, 2017.

Hepach, H., Quack, B., Raimund, S., Fischer, T., Atlas, E. L., and Bracher, A.: Halocarbon emissions and sources in the equatorial Atlantic Cold Tongue, *Biogeosciences*, 12, 6369–6387, <https://doi.org/10.5194/bg-12-6369-2015>, 2015.

Hosking, J.S., Russo, M.R., Braesicke, P. and Pyle, J.A.: Tropical convective transport and the Walker circulation, *Atmos. Chem. Phys.*, 12, 9791–9797, doi: 10.5194/acp-12-9791-2012, 2012.

Hossaini, R., Patra, P.K., Leeson, A.A., Krysztofciak, G., Abraham, N.L., Andrews, S.J., Archibald, A.T., Aschmann, J., Atlas, E.L., Belikov, D.A., Bönisch, H., Carpenter, L.J., Dhomse, S., Dorf, M., Engel, A., Feng, W., Fuhlbrügge, S., Griffiths, P.T., Harris, N.R.P., Hommel, R., Keber, T., Krüger, K., Lennartz, S.T., Maksyutov, S., Mantle, H., Mills, G.P., Miller, B., Montzka, S.A., Moore, F., Navarro, M.A., Oram, D.E., Pfeilsticker, K., Pyle, J.A., Quack, B., Robinson, A.D., Saikawa, E., Saiz-Lopez, A., Sala, S., Sinnhuber, B.-M., Taguchi, S., Tegtmeier, S., Lidster, R.T., Wilson, C., and Ziska, F.: A multi-model intercomparison of halogenated very short-lived substances (TransCom-VSLS): linking oceanic emissions and tropospheric transport for a reconciled estimate of the stratospheric source gas injection of bromine, *Atmos. Chem. Phys.*, 16(14), 9163–9187, doi:10.5194/acp-16-9163-2016, 2016.

Hossaini, R., Chipperfield, M., Montzka, S.A., Leeson, A.A., Dhomse, S.S., and Pyle, J.A.: The increasing threat to stratospheric ozone from dichloromethane, *Nature Comms.*, doi: 10.1038/ncomms15962, 2017.

Jensen, E.J., Pfister, L., Jordan, D.E., Bui, T.V., Ueyama, R., Singh, H.B., Thornberry, T.D., Rollins, A.W., Gao, R., Fahey, D.W., Rosenlof, K.H., Elkins, J.W., Diskin, G.S., DiGangi, J.P., Lawson, R.P., Woods, S., Atlas, E.L., Navarro Rodriguez, M.A., Wofsy, S.C., Pittman, J., Bardeen, C.G., Toon, O.B., Kindel, B.C., Newman, P.A., McGill, M.J., Hlavka, D.L., Lait, L.R., Schoeberl, M.R., Bergman, J.W., Selkirk, H.B., Alexander, M.J., Kim, J.-E., Lim, B.H., Stutz, J., and Pfeilsticker, K.: The NASA Airborne Tropical Tropopause Experiment: High-Altitude Aircraft Measurements in the Tropical Western Pacific, *Bull. Amer. Meteor. Soc.*, 98, 129–143, doi:10.1175/BAMS-D-14-00263.1, 2017.

Jones, A., Thomson, D., Hort, M., and Devenish, B.: The U.K. Met Office's Next-Generation Atmospheric Dispersion Model, NAME III Air Pollution Modeling and Its Application XVII, Springer US, 580–589, doi: 10.1007/978-0-387-68854-1_62, 2007.

Krzysztofciak, G., Catoire, V., Hamer, P.D., Marécal, V., Robert, C., Engel, A., Bönisch, H., Grossman, K., Quack, B., Atlas, E. and Pfeilsticker, K.: Evidence of convective transport in tropical West Pacific region during SHIVA experiment, *Atmos. Sci. Lett.*, 19, 1–7, doi: 10.1002/asl.798, 2018.

Formatted: Font: 12 pt, Font color: Text 1

Formatted: Font: 12 pt

728 Liang, Q., Stolarski, R.S., Kawa, S.R., Nielsen, J.E., Douglass, A.R., Rodriguez, J.M., Blake, D.R.,
 729 Atlas, E.L., and Ott, L.E.: Finding the missing stratospheric Br_y: a global modelling study of CHBr₃
 730 and CH₂Br₂, *Atmos. Chem. Phys.*, 10, 2269-2286, doi: 10.5194/acp-10-2269-2010, 2010.

731 Liang, Q., Atlas, E., Blake, D., Dorf, M., Pfeilsticker, K. and Schauffler, S.: Convective transport of
 732 very short-lived bromocarbons to the stratosphere, *Atmos. Chem. Phys. Discuss.*, 14, 651-676, doi:
 733 10.5194/acpd-14-651-2014, 2014.

734 Lovelock, J.E.: Natural halocarbons in the air and in the sea, *Nature*, 256, 193-194, doi:
 735 10.1038/256193a0, 1975.

736 Meneguz, E. and Thomson, D.J.: Towards a new scheme for parametrization of deep convection in
 737 NAME III, *Int. J. Environ. Pollut.*, 54, 128-136, doi: 10.1504/IJEP.2014.065113, 2014.

738 Meneguz, E., Thomson, D.J., Witham, C., Filus, M.T., Harris, N.R.P., Navarro, M. and Atlas, E.:
 739 Improved parameterisation scheme to represent tropospheric moist convection in NAME, (in
 740 review).

741 Moore, R. M., Geen, C. E., and Tait, V. K.: Determination of Henry Law constants for a suite of
 742 naturally-occurring halo- genated methanes in seawater, *Chemosphere*, 30, 1183–1191, 1995.

743 Navarro, M.A., Atlas, E.A., Saiz-Lopez, A., Rodriguez-Lloveras, X., Kinnison, D.E., Lamarque, J.-
 744 F., Tilmes, S., Filus, M., Harris, N.R.P., Meneguz, E., Ashfold, M.J., Manning, A.J., Cuevas, C.A.,
 745 Schauffler, S.M., and Donets, V.: Airborne measurements of organic bromine compounds in the
 746 Pacific tropical tropopause layer, *PNAS*, USA, 112, 13789-13793, doi: 10.1073/pnas.1511463112,
 747 2015.

748

749 Newton, R., Vaughan, G., Hints, E., Filus, M.T., Pan, L.L., Honomichl, S., Atlas, E., Andrews, S.J.,
 750 and Carpenter, L.J.: Observations of ozone-poor air in the tropical tropopause layer, *Atmos. Chem.*
 751 *Phys.*, 18, 5157-5171, doi:10.5194/acp-18-5157-2018, 2018.

752

753 Oram, D.E. and Penkett, S.A.: Observations in eastern England of elevated methyl iodide
 754 concentrations in air of Atlantic origin, *Atmos. Environ.*, 28, 1159-1174, doi: 10.1016/1352-
 755 2130(94)90293-3, 1994.

756

757 Oram, D.E., Ashfold, M.J., Laube, J.C., Gooch, L.J., Humphrey, S., Sturges, W.T., Leedham-
 758 Elvidge, E., Forster, G.L., Harris, N.R.P., Mead, M.I., Samah, A.A., Phang, S.M., Ou-Yang, C.-F.,
 759 Lin, N.-H., Wang, J.-L., Baker, A.K., Brenninkmeijer, C.A.M., and Sherry, D.: A growing threat to
 760 the ozone layer from short-lived anthropogenic chlorocarbons, *Atmos. Chem. Phys.*, 17, 11929-
 761 11941, doi: 10.5194/acp-17-11929-2017, 2017.

762 Pan, L.L., Atlas, E.L., Salawitch, R.J., Honomichl, S.B., Bresch, J.F., Randel, W.J., Apel, E.C.,
 763 Hornbrook, R.S., Weinheimer, A.J., Anderson, D.C., Andrews, S.J., Baidar, S., Beaton, S.P.,
 764 Campos, T.L., Carpenter, L.J., Chen, D., Dix, B., Donets, V., Hall, S.R., Hanisco, T.F., Homeyer,
 765 C.R., Huey, L.G., Jensen, J.B., Kaser, L., Kinnison, D.E., Koenig, T.K., Lamarque, J., Liu, C., Luo,
 766 J., Luo, Z.J., Montzka, D.D., Nicely, J.M., Pierce, R.B., Riemer, D.D., Robinson, T., Romashkin, P.,
 767 Saiz-Lopez, A., Schauffler, S., Shieh, O., Stell, M.H., Ullmann, K., Vaughan, G., Volkamer, R., and
 768 Wolfe, G.: The Convective Transport of Active Species in the Tropics (CONTRAST) Experiment,
 769 *Bull. Amer. Meteor. Soc.*, 98, 106–128, doi:10.1175/BAMS-D-14-00272.1, 2017.

770 Park, S., Atlas, E.L., Jiménez, R., Daube, B.C., Gottlieb, E.W., Nan, J., Jones, D.B.A., Pfister, L.,
 771 Conway, T.J., Bui, T.P., Gao, R.-S., and Wofsy, S.C.: Vertical transport rates and concentrations of
 772 OH and Cl radicals in the Tropical Tropopause Layer from observations of CO₂ and halocarbons:
 773 implications for distributions of long- and short-lived chemical species, *Atmos. Chem. Phys.*, 10,
 774 6669-6684, doi: 10.5194/acp-10-6669-2010, 2014.

Formatted: Font: Times New Roman, 12 pt

Formatted: Space After: 3 pt

Formatted: Font: 12 pt

Pfeilsticker, K., Sturges, W.T., Bosch, H., Camy-Peyret, C., Chipperfield, M.P., Engel, A.,
 Fitzenberger, R., Muller, M., Payan, S., and Sinnhuber, B.-M.: Lower stratospheric organic and
 inorganic bromine budget for the arctic winter 1998/1999, *Geophys. Res. Lett.*, 27, 3305-3308, doi:
 10.1029/2000GL011650, 2000.
 Pyle, J.A., Ashfold, M.J., Harris, N.R.P., Robinson, A.D., Warwick, N.J., Carver, G.D., Gostlow, B.,
 O'Brien, L.M., Manning, A.J., Phang, S.M., Yong, S.E., Leong, K.P., Ung, E.H., and Ong, S.:
 Bromoform in the tropical boundary layer of the Maritime Continent during OP3, *Atmos. Chem.*
Phys., 11, 529-542, doi: 10.5194/acp-11-529-2011, 2011.
 Russo, M.R., Marécal, V., Hoyle, C.R., Arteta, J., Chemel, C., Chipperfield, M.P., Dessens, O.,
 Feng, W., Hosking, J.S., Telford, P.J., Wild, O., Yang, X., and Pyle, J.A.: Representation of deep
 convection in atmospheric models – Part 1: Meteorology and comparison with satellite observations,
Atmos. Chem. Phys., 11, 2765-2786, doi: 10.5194/acp-11-2765-2011, 2011.
 Russo, M.R., Ashfold, M.J., Harris, N.R.P., and Pyle, J.A.: On the emissions and transport of
 bromoform: sensitivity to model resolution and emission location, *Atmos. Chem. Phys.*, 15, 14031-
 14040, doi: 10.5194/acp-15-14031-2015, 2015.
 Saiz-Lopez, A., Fernandez, R.P., Ordóñez, C., Kinnison, D.E., Gómez-Martin, J.C., Lamarque, J.-F.,
 and Tilmes, S.: Iodine chemistry in the troposphere and its effects on ozone, *Atmos. Chem. Phys.*,
 14, 13119-13143, doi: 10.5194/acp-14-13119-2014, 2014.
 Sala, S., Bönisch, H., Keber, T., Oram, D.E., Mills, G., and Engel, A.: Deriving an atmospheric
 budget of total organic bromine using airborne in situ measurements from western Pacific area
 during SHIVA, *Atmos. Chem. Phys.*, 14, 6903-6923, doi:10.5194/acp-14-6903-2014, 2014.
 Schauffler, S.M., Atlas, E.L., Flocke, F., Lueb, R.A., Stroud, V., and Travnicek, W.: Measurements
 of bromine containing organic compounds at the tropical tropopause, *Geophys. Res. Lett.*, 25, 3, 317-
 320, doi:10.1029/98GL00040, 1998.
 Schofield, R., Fueglistaler, S., Wohltmann, I., and Rex, M.: Sensitivity of stratospheric BrO to
 uncertainties in very short lived substance emissions and atmospheric transport, *Atmos. Chem.*
Phys., 11, 1379-1392, doi:10.5194/acp-11-1379-2011, 2011.
 Solomon, S., Garcia, R.R., and Ravishankara, A.R.: On the role of iodine in ozone depletion, *J.*
Geophys. Res., 99, 20941, doi: 10.1029/94JD02028, 1994.
 Steinbrecht, W., Froidevaux, L., Fuller, R., Wang, R., Anderson, J., Roth, C., Bourassa, A.,
 Degenstein, D., Damadeo, R., Zawodny, J., Frith, S., McPeters, R., Bhartia, P., Wild, J., Long, C.,
 Davis, S., Rosenlof, K., Sofieva, V., Walker, K., Rahpoe, N., Rozanov, A., Weber, M., Laeng, A.,
 von Clarmann, T., Stiller, G., Kramarova, N., Godin-Beekmann, S., Leblanc, T., Querel, R., Swart,
 D., Boyd, I., Hocke, K., Kämpfer, N., Maillard Barras, E., Moreira, L., Nedoluha, G., Vigouroux, C.,
 Blumenstock, T., Schneider, M., García, O., Jones, N., Mahieu, E., Smale, D., Kotkamp, M.,
 Robinson, J., Petropavlovskikh, I., Harris, N., Hassler, B., Hubert, D., and Tummon, F.: An update
 on ozone profile trends for the period 2000 to 2016, *Atmos. Chem. Phys.*, 17, 10675– 10690, doi:
 10.5194/acp-17-10675-2017, 2017.
 Tegtmeier, S., Krüger, K., Quack, B., Atlas, E.L., Pissio, I., Stohl, A., and Yang, X.: Emission and
 transport of bromocarbons: from the West Pacific ocean into the stratosphere, *Atmos. Chem. Phys.*,
 12, 10633-10648, doi: 10.5194/acp-12-10633-2012, 2012.
 Tegtmeier, S., Krüger, K., Quack, B., Atlas, E., Blake, D.R., Boenish, H., Engel, A., Hepach, H.,
 Hossaini, R., Navarro, M.A., Raimund, S., Sala, S., Shi, Q., and Ziska, F.: The contribution of
 oceanic methyl iodide to stratospheric iodine, *Atmos. Chem. Phys.*, 13, 11869-11886, doi:
 10.5194/acp-13-11869-2013, 2013.
 Tegtmeier, S., Ziska, F., Pissio, I., Quack, B., Velders, G.J.M., Yang, X., and Krüger, K.: Oceanic
 bromoform emissions weighted by their ozone depletion potential, *Atmos. Chem. Phys.*, 15, 13647-
 13663, doi: 10.5194/acp-15-13647-2015, 2015.

823 Vogt, R., Sander, R., von Glasow, R. and Crutzen, P.J.: Iodine chemistry and its role in halogen
824 activation and ozone loss in the marine boundary layer: a model study, *J. Atmos. Chem.*, 32, 375-
825 395, doi: 10.1023/A:1006179901037, 1999.

826 Wales, P.A., Salawitch, R.J., Nicely, J.M., Anderson, D.C., Canty, T.P., Baidar, S., et al.:
827 Stratospheric injection of brominated very short-lived substances: aircraft observations in the
828 Western Pacific and representation in global models., *Journal of Geophysical Research:*
829 *Atmospheres*, 123, 5690-5719, <https://doi.org/10.1029/2017.JD027978>, 2018.

830 Walters, D., Baran, A. J., Boutle, I., Brooks, M., Earnshaw, P., Edwards, J., Furtado, K., Hill, P.,
831 Lock, A., Manners, J., Morcrette, C., Mulcahy, J., Sanchez, C., Smith, C., Stratton, R., Tennant, W.,
832 Tomassini, L., Van Weverberg, K., Vosper, S., Willett, M., Browse, J., Bushell, A., Carslaw, K.,
833 Dalvi, M., Essery, R., Gedney, N., Hardiman, S., Johnson, B., Johnson, C., Jones, A., Jones, C.,
834 Mann, G., Milton, S., Rumbold, H., Sellar, A., Ujiie, M., Whittall, M., Williams, K., and Zerroukat,
835 M.: The Met Office Unified Model Global Atmosphere 7.0/7.1 and JULES Global Land 7.0
836 configurations, *Geosci. Model Dev.*, 12, 1909—1963, doi: 10.5194/gmd-12-1909-2019, 2019.

837

838 Wang, S., Schmidt, J.A., Baidar, S., Coburn, S., Dix, B., Koenig, T.K., Apel, E., Bowdalo, D.,
839 Campos, T.L., Eloranta, E., Evans, M.J., DiGangi, J.P., Zondlo, M.A., Gao, R.S., Haggerty, J.A.,
840 Hall, S.R., Hornbrook, R.S., Jacob, D., Morley, B., Pierce, B., Reeves, M., Romashkin, P., Ter
841 Schure A., and Volkamer, R.:Active and widespread halogen chemistry in the tropical and
842 subtropical free troposphere, *PNAS*, 112 (30), 9281-9286, doi:10.1073/pnas.1505142112, 2015.

843 Yang, G.P., Yang, B., Lu, X.L: Spatio-temporal variations of sea surface halocarbon concentrations
844 and fluxes from southern Yellow Sea.- *Biogeochemistry*, 121: 369. [https://doi.org/10.1007/s10533-](https://doi.org/10.1007/s10533-014-0007-x)
845 [014-0007-x](https://doi.org/10.1007/s10533-014-0007-x), 2014.

846

847

Formatted: Font: 12 pt, Font color: Text 1

Formatted: Font color: Text 1

Formatted: Font: 12 pt, Font color: Text 1

Formatted: Font: 12 pt, Font color: Text 1

Formatted: Font color: Text 1

Formatted: Font: 12 pt, Font color: Text 1

Formatted: Font: 12 pt

848
849
850
851

11 Tables

Table 1. Boundary layer concentrations and atmospheric lifetimes for CH₃I, CHBr₃ and CH₂Br₂ (Carpenter et.al., 2014).

Tracer, [X]	Boundary Layer Concentration, [X] _{BL} [ppt]		Atmospheric Lifetime, τ [days]
	CAST and CONTRAST	Carpenter et al., 2014	
	Mean (Range) Median	Median (Range)	
CH ₃ I	0.70 (0.16-3.34) 0.65	0.8 (0.3-2.1)	4
CHBr ₃	0.83 (0.41-2.56) 0.73	1.6 (0.5-2.4)	15
CH ₂ Br ₂	0.90 (0.61-1.38) 0.86	1.1 (0.7-1.5)	94

852
853
854
855
856
857

Table 2. ATTREX 2014 Research Flight 02: AWAS observations, modelled boundary layer contribution, the modelled total mixing ratios for CH₃I, CHBr₃ and CH₂Br₂. The boundary layer and background fractions means and standard deviations (in brackets) are given based on the measurements and modelled values for the samples collected during the flight.

Altitude [km]	AWAS [ppt]	Modelled Boundary Layer Contribution [ppt]	Modelled Total Mixing Ratio [ppt]
CH₃I			
17-18	0.06 (0.02)	0.00 (0.00)	0.06 (0.02)
16-17	0.09 (0.03)	0.00 (0.00)	0.06 (0.02)
15-16	0.17 (0.03)	0.04 (0.04)	0.12 (0.06)
14-15	0.23 (0.09)	0.17 (0.04)	0.21 (0.08)
CHBr₃			
17-18	0.34 (0.17)	0.01 (0.00)	0.29 (0.15)
16-17	0.42 (0.11)	0.03 (0.01)	0.36 (0.14)
15-16	0.55 (0.06)	0.12 (0.07)	0.48 (0.17)
14-15	0.67 (0.10)	0.35 (0.07)	0.58 (0.13)
CH₂Br₂			
17-18	0.72 (0.02)	0.02 (0.01)	0.71 (0.03)
16-17	0.79 (0.07)	0.06 (0.02)	0.76 (0.06)
15-16	0.83 (0.05)	0.19 (0.09)	0.78 (0.10)
14-15	0.89 (0.05)	0.46 (0.08)	0.84 (0.12)
Boundary Layer fraction [%]		Background fraction [%]	
17-18	2.1 (1.1)	97.9	
16-17	7.2 (2.7)	92.8	
15-16	22.9 (10.0)	77.1	
14-15	53.3 (9.0)	46.7	

858
859
860
861
862

Table 3. ATTREX 2014 all flights: AWAS observations, modelled boundary layer contribution, the modelled total mixing ratios for CH₃I, CHBr₃ and CH₂Br₂. The boundary layer and background fractions are also given. Means and standard deviations (in brackets).

Altitude [km]	AWAS [ppt]	Modelled Boundary Layer Contribution	Modelled Total Mixing Ratio [ppt]
------------------	---------------	---	--------------------------------------

	[ppt]		
CH₃I			
17-18	0.04 (0.03)	0.02 (0.03)	0.07 (0.04)
16-17	0.11 (0.10)	0.04 (0.04)	0.09 (0.05)
15-16	0.16 (0.14)	0.09 (0.07)	0.15 (0.08)
14-15	0.17 (0.14)	0.15 (0.08)	0.19 (0.11)
CHBr₃			
17-18	0.33 (0.14)	0.06 (0.06)	0.32 (0.16)
16-17	0.48 (0.13)	0.12 (0.09)	0.40 (0.17)
15-16	0.54 (0.13)	0.21 (0.12)	0.50 (0.19)
14-15	0.61 (0.13)	0.31 (0.12)	0.55 (0.16)
CH₂Br₂			
17-18	0.73 (0.06)	0.11 (0.09)	0.73 (0.09)
16-17	0.82 (0.08)	0.19 (0.14)	0.78 (0.15)
15-16	0.84 (0.09)	0.32 (0.16)	0.80 (0.17)
14-15	0.86 (0.07)	0.44 (0.15)	0.84 (0.17)
	Boundary Layer fraction [%]	Background fraction [%]	
17-18	12.7 (10.9)	87.3	
16-17	22.3 (16.0)	77.7	
15-16	37.8 (18.8)	62.2	
14-15	51.7 (16.1)	48.3	

Table 4. ATTREX 2013 all flights: AWAS observations, modelled boundary layer contribution, the modelled total mixing ratios for CH₃I, CHBr₃ and CH₂Br₂. The boundary layer and background fractions are also given. Means and standard deviations (in brackets).

Altitude [km]	AWAS [ppt]	Modelled Boundary Layer Contribution [ppt]	Modelled Total Mixing Ratio [ppt]
CH₃I			
17-18	0.03 (0.02)	0.00 (0.00)	0.03 (0.01)
16-17	0.03 (0.02)	0.00 (0.00)	0.03 (0.02)
15-16	0.04 (0.02)	0.01 (0.01)	0.03 (0.03)
14-15	0.04 (0.03)	0.01 (0.01)	0.05 (0.03)
CHBr₃			
17-18	0.31 (0.10)	0.01 (0.01)	0.31 (0.09)
16-17	0.39 (0.12)	0.02 (0.02)	0.35 (0.11)
15-16	0.54 (0.15)	0.04 (0.04)	0.49 (0.16)
14-15	0.53 (0.15)	0.07 (0.05)	0.53 (0.18)
CH₂Br₂			
17-18	0.79 (0.08)	0.02 (0.04)	0.78 (0.07)
16-17	0.83 (0.07)	0.04 (0.04)	0.81 (0.07)
15-16	0.90 (0.07)	0.07 (0.06)	0.87 (0.10)
14-15	0.91 (0.08)	0.12 (0.09)	0.89 (0.12)
	Boundary Layer fraction [%]	Background fraction [%]	

17-18	1.9 (2.3)	98.1
16-17	4.7 (4.9)	95.3
15-16	9.8 (7.9)	90.2
14-15	14.7 (11.1)	85.3

Table 5. Contribution from the very short-lived bromocarbons: CHBr_3 and CH_2Br_2 to the bromine in the TTL as given by modelled estimates and AWAS observations for ATTREX 2014 and 2013. $[\text{CHBr}_3]$ and $[\text{CH}_2\text{Br}_2]$ means are shown only.

Altitude [km]	$[\text{CHBr}_3]$ [ppt]	$[\text{CH}_2\text{Br}_2]$ [ppt]	Br from CHBr_3 [ppt]	Br from CH_2Br_2 [ppt]	Br-VSL _{org} [ppt]
ATTREX 2014					
NAME					
17-18	0.32	0.73	0.96	1.46	2.42
16-17	0.40	0.78	1.20	1.56	2.76
15-16	0.50	0.80	1.50	1.60	3.10
14-15	0.55	0.84	1.65	1.68	3.33
AWAS					
17-18	0.33	0.73	0.99	1.46	2.45
16-17	0.48	0.82	1.44	1.64	3.08
15-16	0.54	0.84	1.62	1.68	3.30
14-15	0.61	0.86	1.83	1.72	3.55
ATTREX 2013					
NAME					
17-18	0.31	0.78	0.93	1.56	2.49
16-17	0.35	0.81	1.05	1.62	2.67
15-16	0.49	0.87	1.47	1.74	3.21
14-15	0.53	0.89	1.59	1.78	3.37
AWAS					
17-18	0.31	0.79	0.93	1.58	2.51
16-17	0.39	0.83	1.17	1.66	2.83
15-16	0.54	0.90	1.62	1.80	3.42
14-15	0.53	0.91	1.59	1.82	3.41

12 Figures

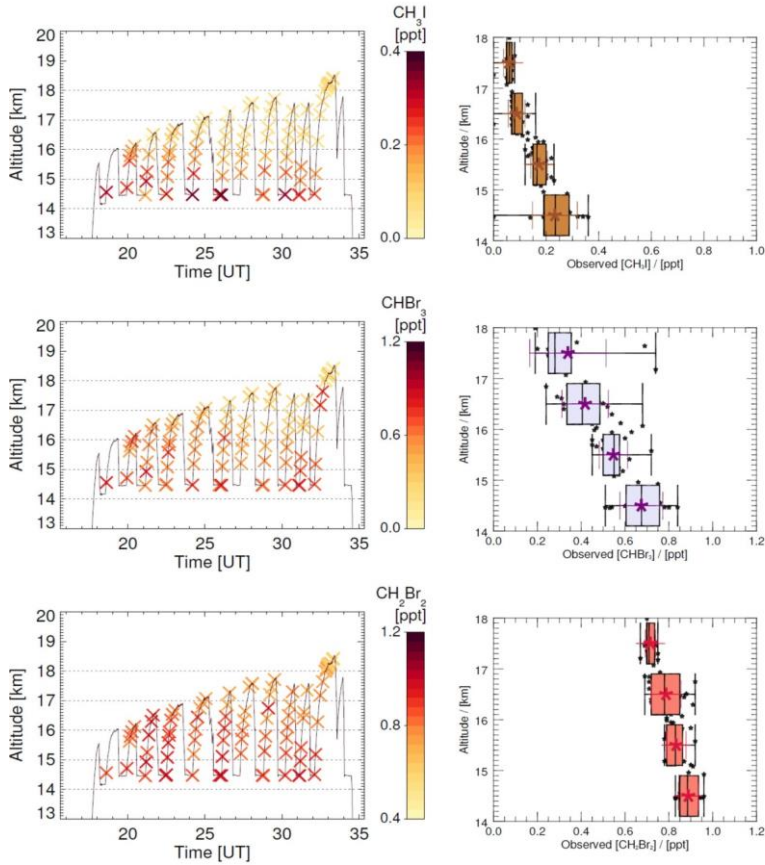


Figure 1: Vertical distribution of CH_3I , CHBr_3 and CH_2Br_2 in the TTL, as measured during Research Flight 02, ATTREX 2014: AWAS measurements along the flight track (left), observations grouped into 1 km TTL segments (right): means (star symbols), standard deviations (coloured whiskers), minimum, lower and upper quartiles, median and maximum (black box and whiskers). Vertical distribution of CH_3I , CHBr_3 and CH_2Br_2 in the TTL, as measured during Research Flight 02, ATTREX 2014: AWAS measurements along the flight track (left), observations grouped into 1 km TTL segments (right, means (star symbols), standard deviations (coloured whiskers), minimum, lower and upper quartiles, median and maximum (black box and whiskers)).

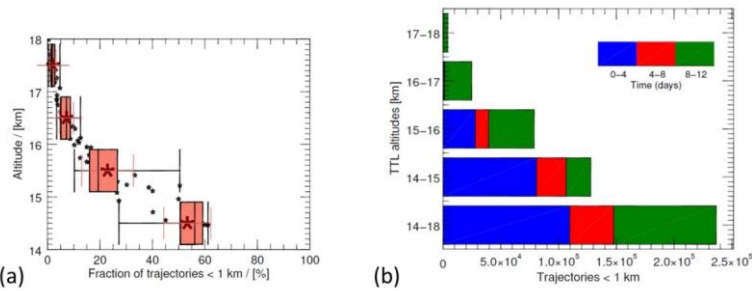


Figure 2: Vertical distribution of NAME 1 km fractions (the fractions which reach the boundary layer within 12 days - indicative of boundary layer air influence) in the TTL (2a, left). Distribution of transport times taken for the trajectories

to first cross below 1 km (reach boundary layer) for all the NAME runs and the NAME runs grouped into 1 km TTL segments, [Research Flight 02](#), ATTREX 2014 (2b, right).

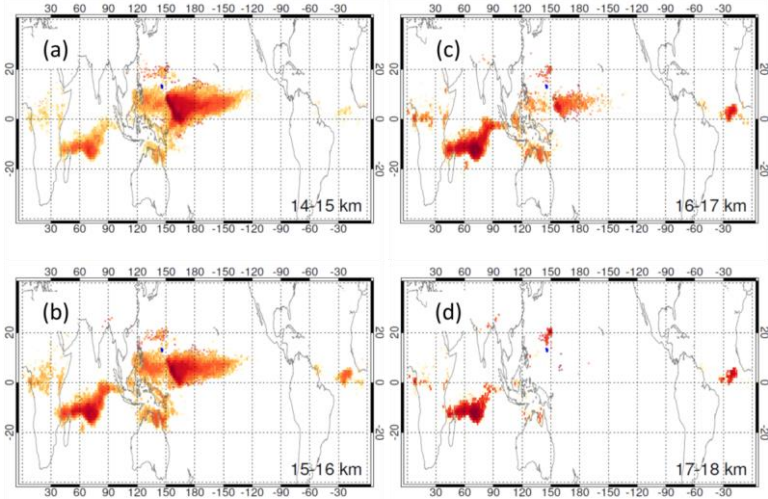


Figure 3: Crossing location distribution maps for all the NAME runs released from 4 1 km TTL altitudes: 14-15 km. Strong influence of local boundary air is noted for a 14-15 km segment (lower TTL), whereas the boundary air from remote locations dominates for a 17-18 km segment (upper TTL), [research flight Research Flight 02](#), ATTREX 2014.

Formatted: Font: 10 pt

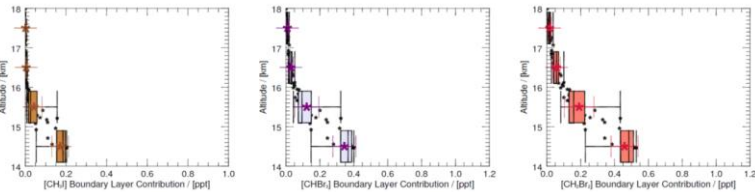


Figure 4: NAME modelled CH_3I , CHBr_3 and CH_2Br_2 boundary layer contribution to the TTL, [research flight Research Flight 02](#), ATTREX 2014.

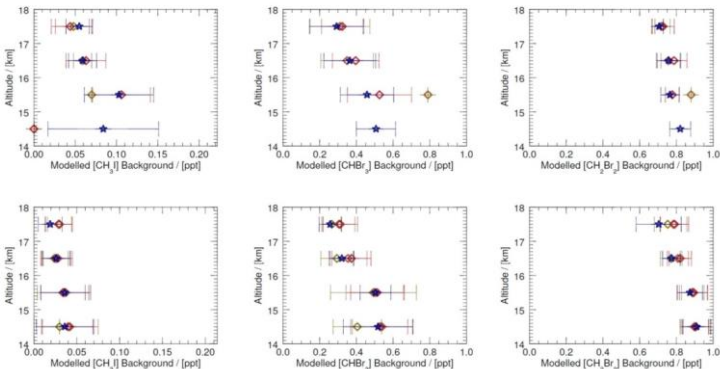


Figure 5: Background mixing ratios for CH_3I , CHBr_3 and CH_2Br_2 for all NAME runs for all flights in ATTREX 2014 (top row) and ATTREX 2013 (bottom row). Little convective influence is indicated by selecting means from NAME 1 km fractions of <1 (blue star), 5 (red diamond) and 10 (green diamond) %.

903
904
905
906

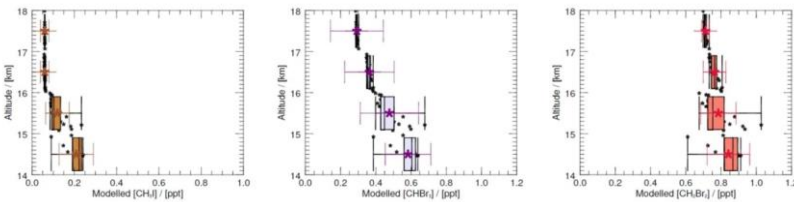


Figure 6: Vertical distribution of NAME modelled CH_3I , CHBr_3 and CH_2Br_2 (sums of boundary layer and background contribution) in the TTL for [research flight](#) Research Flight 02, ATTREX 2014.

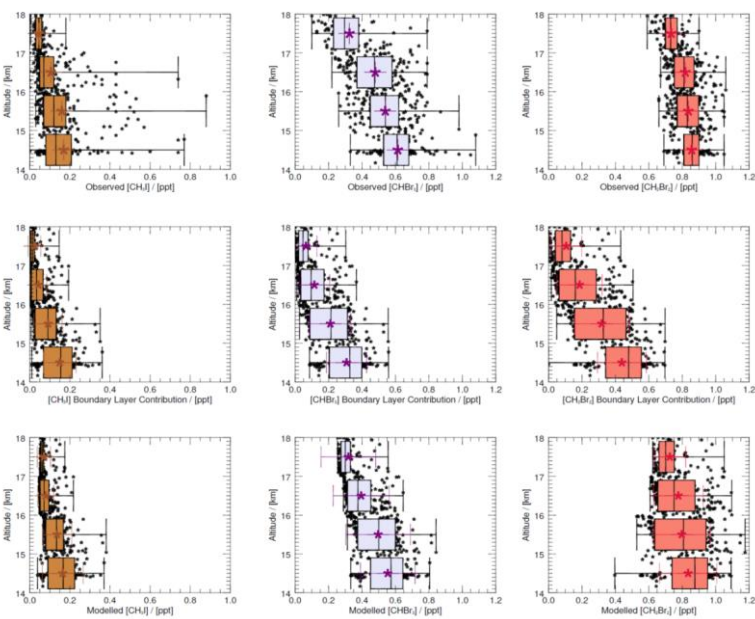


Figure 7: CH_3I , CHBr_3 and CH_2Br_2 vertical distribution in the TTL for ATTREX 2014 flights: AWAS observations (top row), NAME modelled boundary layer contribution (middle row), and NAME modelled sums of boundary layer and background contributions (bottom row).

907
908
909
910
911
912

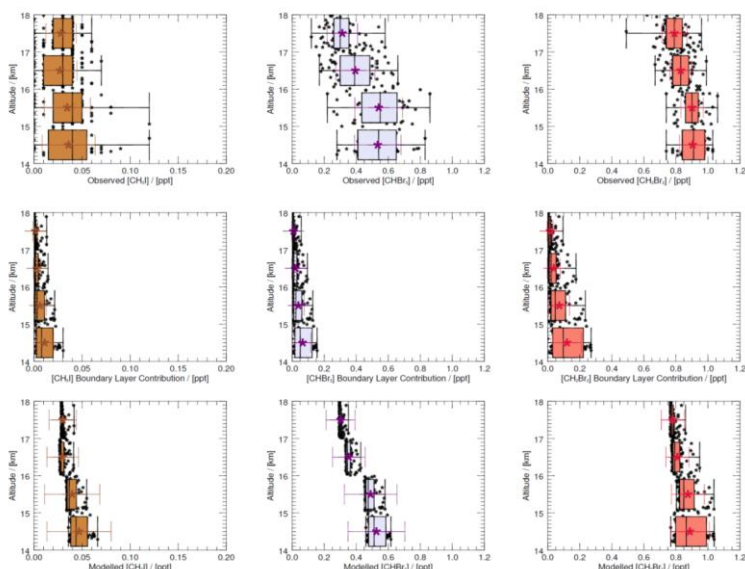


Figure 8: CH_3I , CHBr_3 and CH_2Br_2 vertical distribution in the TTL for ATTREX 2013 flights: AWAS observations (top row), NAME modelled boundary layer contribution (middle row), and NAME modelled sums of boundary layer and background contributions (bottom row).

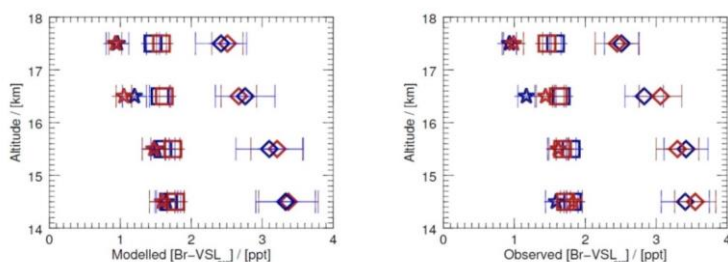


Figure 9: Contribution of CHBr_3 (star symbol) and CH_2Br_2 (square symbol) to the bromine budget in the TTL, inferred from the NAME modelled estimates (left) and AWAS observations (right); separately ATTREX 2014 (red) and 2013 (blue). Star and square symbols represent the bromine atomicity products from CHBr_3 and CH_2Br_2 , respectively. Diamonds show the bromine contribution from the VSL bromocarbons in the TTL (as a sum of the CHBr_3 and CH_2Br_2 bromine atomicity products).